



Stockholm  
University

# Bachelor Thesis

Degree Project in  
Geology 30 hp

## **A study of the evidence for glacial/interglacial cyclicality within the Port Askaig Formation, Port Askaig, Islay**

Joe Browning



Stockholm 2018

Department of Geological Sciences  
Stockholm University  
SE-106 91 Stockholm  
Sweden

## Abstract

The aim of this study is to evaluate the evidence for cyclicity within the Port Askaig Formation, Port Askaig, Islay, Scotland. A sedimentary log of a 4 km section of the formation was prepared to document all field evidence of shifting climatic conditions, noting each glacial, interglacial or periglacial layer. The outcropped layers were found to occur multiple times across faulting regions and their positioning largely confirms the cyclicity discussed in the paleoclimate archive literature.

One particular 7 m thick interglacial layer was chosen to study in more detail using X-ray fluorescence (XRF) at 2 cm intervals perpendicular to the layering. XRF analysis showed fluctuations in both the manganese concentration and the ratio of potassium to rubidium. These fluctuations, combined with other proxies from the literature, show significant variations in deep ocean oxygenation and terrestrial chemical weathering suggesting additional shifts in climate undocumented in the sedimentary archive of the formation.

## CONTENTS

|   |    |
|---|----|
| Abstract .....  | 2  |
| 1. Introduction .....                                   | 4  |
| 1.1 Snowball Earth Hypothesis.....                      | 6  |
| 1.2 Review of Relevant Proxies. ....                    | 14 |
| 2. Geological background of Port Askaig Formation ..... | 16 |
| 3. Methods.....   | 20 |
| 3.1 Sedimentary log .....                               | 20 |
| 3.2 Handheld XRF method .....                           | 20 |
| 4. Results.....   | 22 |
| 4.1 Sedimentary log .....                               | 22 |
| 4.2 Handheld XRF data .....                             | 25 |
| 4.3 Further Analysis .....                              | 34 |
| 5. Discussion .....                                     | 34 |
| 5.1 Sedimentary log .....                               | 34 |
| 5.2 Handheld XRF data.....                              | 35 |
| 6. Conclusion.....                                      | 38 |
| 7. Acknowledgements.....                                | 39 |
| 8. References .....                                     | 40 |

## 1. INTRODUCTION

The aim of this study is to test the hypothesis that evidence of glacial/interglacial cyclicity can be found within the Port Askaig Formation, an inferred record of the Cryogenian Snowball Earth, on Islay, Scotland. The specific goals of this project are, firstly, to construct a sedimentary log of a 4 km stretch of the Port Askaig Formation, and secondly, to identify any potential cyclicity within these layers by conducting an XRF analysis across a single sandstone between diamictite layers exposed along a roadcut at Port Askaig, Islay. The study area for this project, shown in figures 1 and 2, is a 4 km stretch of the east coast of Islay, geologically speaking, this area is comprised of the Lossit Limestone, overlain by the Port Askaig Formation (PAF), moving up the stratigraphy from the PAF is then the Bonahaven Dolomite Formation. The Port Askaig Formation comprises a sequence of alternating layers of diamictite and sedimentary deposits. Numerous authors (e.g. Ali et al., 2017; Kilburn et al., 1965; Spencer, 1971) have interpreted these layers as glacial and interglacial layers from the Cryogenian period. The Port Askaig Formation will be discussed in detail in section 2.1, while an overview of the Cryogenian Snowball Earth hypothesis is provided in section 1.1 to provide insight into the relevant paleoclimatic details that are pertinent to this study.

The layers of the Port Askaig Formation, outcropping along the coast of Islay, comprise 17 diamictite, 17 interglacial and 27 periglacial layers (Ali et al., 2017). The diamictite layers are interbedded with sandstones, mudstones and carbonate layers as discussed by (Spencer, 1971). The lithology of both clasts and matrix change from predominantly intrabasinal and dolomitic at the base to extra basinal and granitic at the top (Arnaud and Fairchild, 2011). The findings and a complete sedimentary log of the study area is presented in section 4.1.

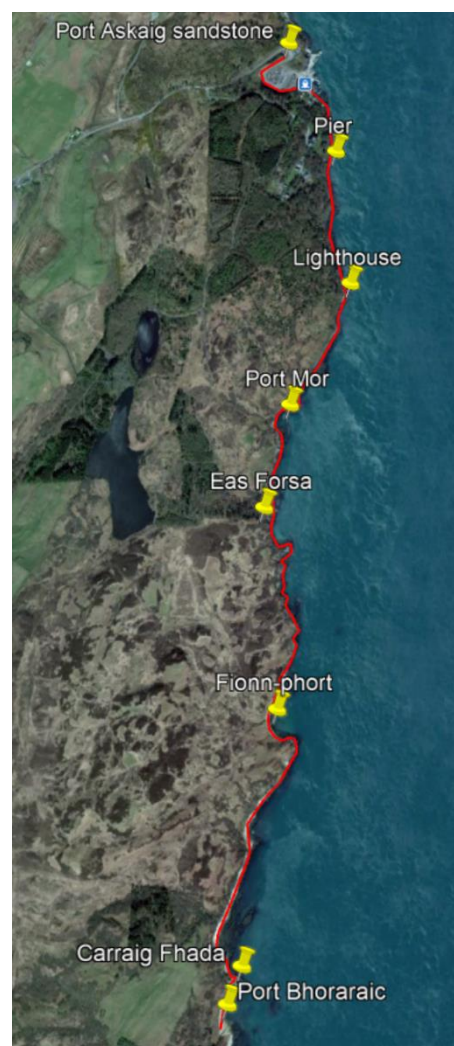


**Figure 1:** Showing the area mapped during the study, produced in Google Earth.

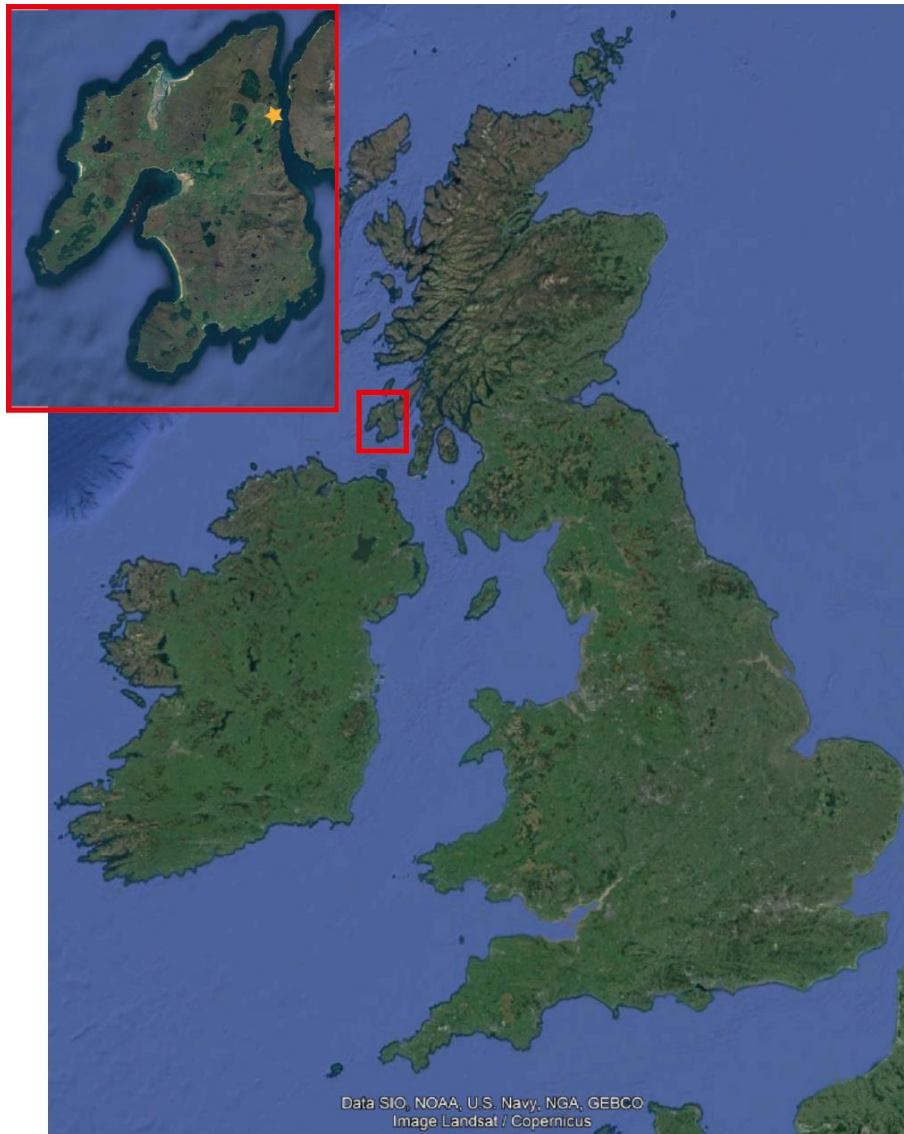


**Figure 2:** Showing the location of Islay within the United Kingdom, the yellow star indicates Port Askaig, the location of the sandstone used for XRF analysis, produced in Google Earth.

The sandstone layer at Port Askaig was identified due to its alternating green and red layers and was selected for further study using XRF analysis. An image of a part of the sandstone can be found in figure 3. Elemental analysis was conducted across the layer to provide further understanding of paleoclimatic conditions during deposition. Furthermore, the data was analysed to identify evidence of cyclicity using a set of climatological proxies (Clift et al., 2014; Jakobsson et al., 2000). A full description and discussion of the data will be found in sections 4.2 and 5.2 respectively while a discussion of climatological proxies occurs in section 1.2.



**Figure 3:** Showing a part of the sandstone layer at 55°50'54.98"N, 6° 6'23.02"W in Port Askaig, Islay displaying distinct red and green banding layers. 30 cm ruler is shown in the image for scale.

## 1.1 Snowball Earth Hypothesis

The Neoproterozoic Era occurred between 1000 Ma and 541 Ma. This era is divided into three periods the Tonian, Cryogenian and Ediacaran (Gradstein and Ogg, 2016). The period of interest for this study is the Cryogenian, occurring between 720 Ma and 635 Ma (Hoffman et al., 2017; Macdonald et al., 2010).

Global geological evidence points to two periods of icehouse conditions during the Neoproterozoic, Cryogenian period, as well as at least one such event during the Proterozoic (Hoffman et al., 2017). The timing of these can be seen in figure 4 retraced and adapted from Hoffman et. al., (2017). The event most relevant to this study is that of the Sturtian glaciation, during the early Cryogenian at approximately 717 - 659 Ma (Hoffman et al., 2017). Another major glacial event occurred around 645-635 Ma and is known as the Marinoan glaciation (Hoffman et al., 2017). The conclusion of this data suggests that the Earth underwent protracted global icehouse conditions twice during the Neoproterozoic, however, there is much debate over the causes and true nature of these glaciations, which will be discussed in the following sections.

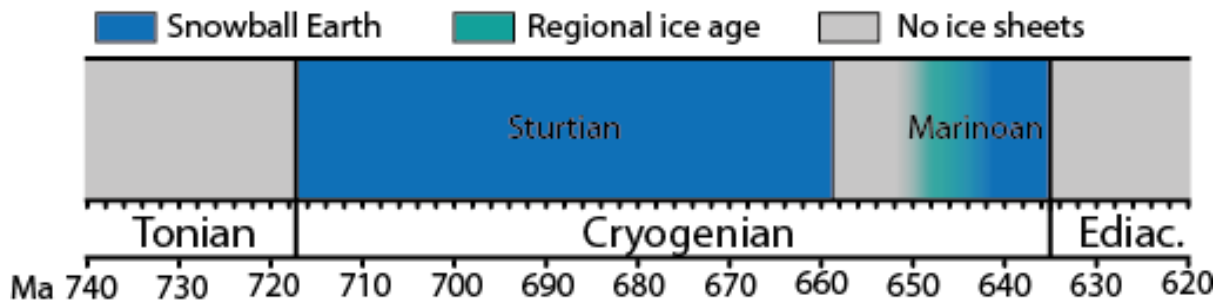


**Figure 4:** Graph showing the age of the Cryogenian period along with the distribution of glaciation and potential snowball occurrences shown in green and blue. Retraced and adapted from (Hoffman et al., 2017)

The Cryogenian was a period of extreme climatic shifts; key to the Snowball Earth hypothesis is the climate forcing conditions that enabled such drastic changes. One factor, not seen on Earth since the Cryogenian, is the distribution of global landmass. At this time there was what Kirschvink called an unusual preponderance of land masses within the middle and low latitudes (Lowe et al., 1992). The predicted distribution of global landmass at this time can be seen in figure 5.

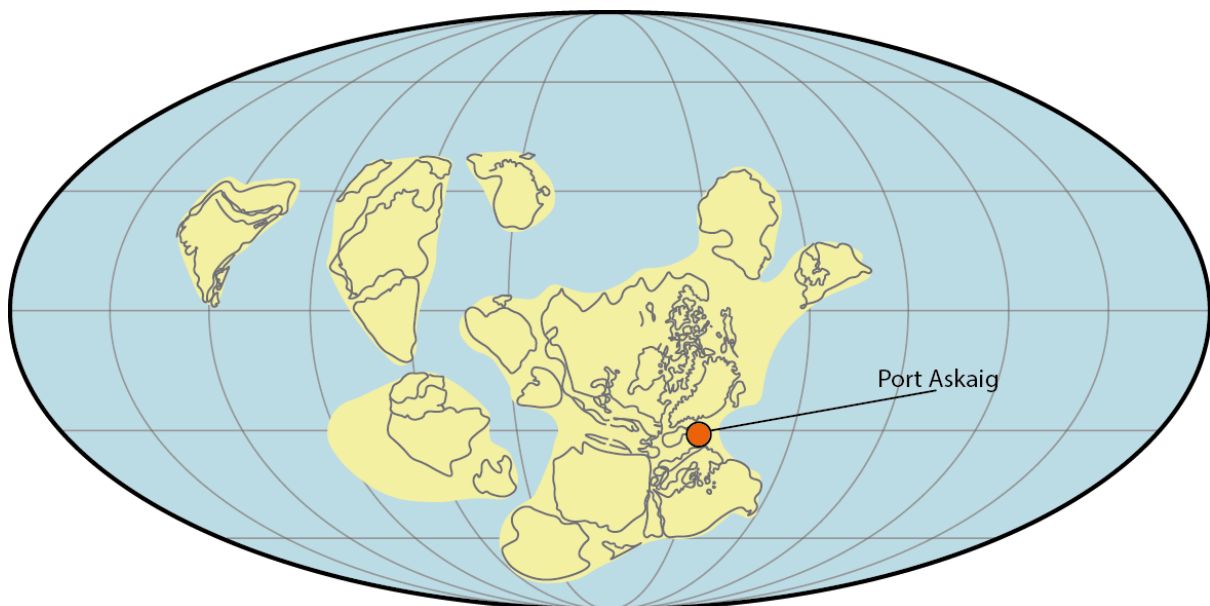


**Figure 5:** Map showing the approximate paleogeography of landmass during the Sturtian glaciation, around 715 Ma. Port Askaig is indicated around 30 degrees south. Retraced and adapted from (Arnaud et al., 2011; Hoffman et al., 2017)

During the Sturtian glaciation (717 - 659 Ma), the supercontinent of Rodinia was located at low latitudes at a time when no land masses occupied the polar regions (Hoffman et al., 2017), as seen in figure 5. This concentration of landmass at low latitudes had the potential to greatly increase planetary albedo, thus decreasing the net insolation of the Earth from solar radiation. A large proportion of the solar energy absorbed by the Earth today, occurs at the surface of tropical oceans, where cloud

coverage has the least mitigating effect. During the Cryogenian, much of this tropical oceanic region was covered with the continental landmass of Rodinia, which has a much higher albedo than seawater or landmasses at higher latitudes (Lowe et al., 1992). Kirschvink also notes that only a small shift in sea level would drain epicontinental seas and expose large areas of reflective continental surface and thus further reduce net insolation.

Snowball hypothesis, as discussed by Schrag et al. (2002) suggests that these paleogeographic landmass distribution conditions would be the catalyst for an increase in global glaciation. The initial impact of this increase in glaciation is twofold. Firstly, in all areas affected by these conditions, the albedo of the Earth's surface increases, thus increasing planetary albedo further. Secondly, sea level is reduced due to water being locked up in ice on land and thus exposing the aforementioned epicontinental seas. As the sea level drops, far more reflective continental surface is exposed contributing even further to planetary albedo (Hoffman and Schrag, 2002; Lowe et al., 1992). Vascular plants did not evolve until the Silurian (443 – 449Ma), meaning the continental surface at this time would not have been covered by foliage, further compounding the reduction in net insolation during this period (Hoffman et al., 2017).

The volume of landmass in the tropics during the Neoproterozoic combined with tectonic uplift would also drastically increase the rate of silicate weathering (Hoffman and Schrag, 2002). During the late Proterozoic, no continental landmass was covered by oceans whilst the average continental latitude is estimated at 21°, (18 ka) (Worsley and Kidder, 1991). This resulted in a drastic increase in the rate of silicate weathering and therefore an increase in the removal of CO<sub>2</sub> from the atmosphere in the form of HCO<sub>3</sub>, later converted to calcium carbonate (CaCO<sub>3</sub>) in the oceans. Schrag, et. al. (2002) note that even a slight imbalance between source and sink over millions of years would strip a vast amount of carbon from the atmosphere (Schrag et al., 2002). As such, when we perceive the period of the Neoproterozoic through the lens of geologic time, we see that, under these conditions, the ocean and atmospheric reservoirs could easily have been depleted of CO<sub>2</sub>. This, in turn, reduced greenhouse conditions and lowered global temperatures to a global average of 7°C compared to the modern average of 15°C (Worsley and Kidder, 1991).

A low latitude landmass on the scale of Rodinia would also cause tropical air to be dryer on average, this would weaken meridional heat transport by Hadley cells and, potentially, also decrease oceanic heat transport. Growth of ice caps bordering polar seas would increase, contributing to ice-albedo feedback (Hoffman and Schrag, 2002).

Neoproterozoic paleoclimate contributions to the Cryogenian glaciations, were also affected by climate feedbacks. The most important feedback considered in this study is ice-albedo. When ice

forms it increases the albedo of the Earth's surface at a given location, this is explained in figure 6, as the migration of ice sheets equatorward reduces total insolation. As sea ice approaches a critical latitude (as it is believed that it did during the Sturtian and Marinoan glaciations) it advances uncontrollably towards the equator due to the spike in planetary albedo (Hoffman et al., 2017; Hoffman and Schrag, 2002). To illustrate the power of this climatological feedback a great deal of analysis has been conducted using general circulation models (GCM). GCMs are a type of climate model used to study the circulation within the atmosphere or oceans (IPCC Data, 2018). These models suggest this final advance of ice towards the equator occurred within 150 years (Lewis et al., 2007), an extremely fast and drastic climatic shift.

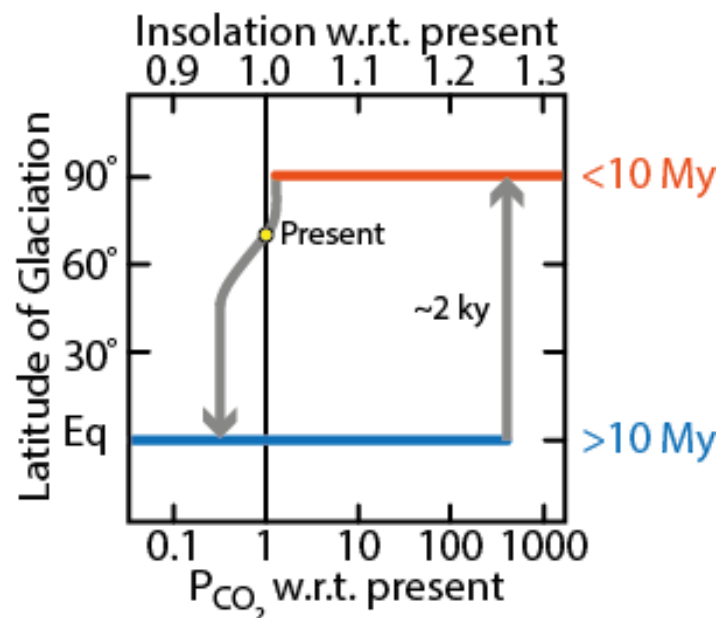


**Figure 6:** Retraced model showing energy balance model of Snowball Earth demonstrating the two points of climatic shift caused by increased albedo from ice cover and increased CO<sub>2</sub> concentration from volcanic activity adapted from (Hoffman et al., 2017).

Negative feedbacks to climate cooling also play a dramatic role in climatic shifts, modelling suggests that land-area feedback can have a moderating effect on cooling through coverage of continental surface via glaciation. As ice progresses from the poles through low latitudinal areas, land is covered thus reducing the availability of rock surfaces for silicate weathering and impeding the further reduction of atmospheric and oceanic CO<sub>2</sub>. The unique characteristic of the glaciations studied here, as mentioned earlier, is the landmass distribution, centred on low latitudes. Because of this, the negative feedback that would normally slow or stop the change in climate is bypassed. (Schrag et al., 2002).

The purpose of the snowball hypothesis, as with any scientific hypothesis, is to resolve a spectrum of evidence into a unified theory. The snowball model manages to explain a wide range of evidence which has not yet been accounted for in other models. The global distribution of late Neoproterozoic glacial deposits (LNGD) were, at the time of their discovery, highly anomalous. The global distribution of these deposits can be seen in figure 7. This distribution is based on palaeomagnetic analysis modified from (Evans, 2000). Not all glacial deposits can be reliably analysed for paleomagnetic data but, of the six deposits judged to have moderate reliability, half formed at a latitude of <math> < 30^\circ </math> and all at a latitude of <math> < 50^\circ </math> (Evans, 2000; Hoffman 2002). LNGD have been found on all continents, displaying the widest possible distribution (Evans, 2000). We also find, at a global level, LNGD to be overlaid by distinctive conformable carbonate cap layers, suggesting a sudden shift in paleoclimate occurring abruptly after glaciation (Hoffman and Schrag, 2002). While the data discussed here for paleogeographic distribution of LNGD is not conclusive, we can conclude that significant evidence exists for low latitude landmass for the period while no evidence is yet available for any high latitude landmass. This conclusion also correlates with aspects of the snowball hypothesis that rely on low latitude land distribution as a catalyst for glaciation and icehouse conditions.

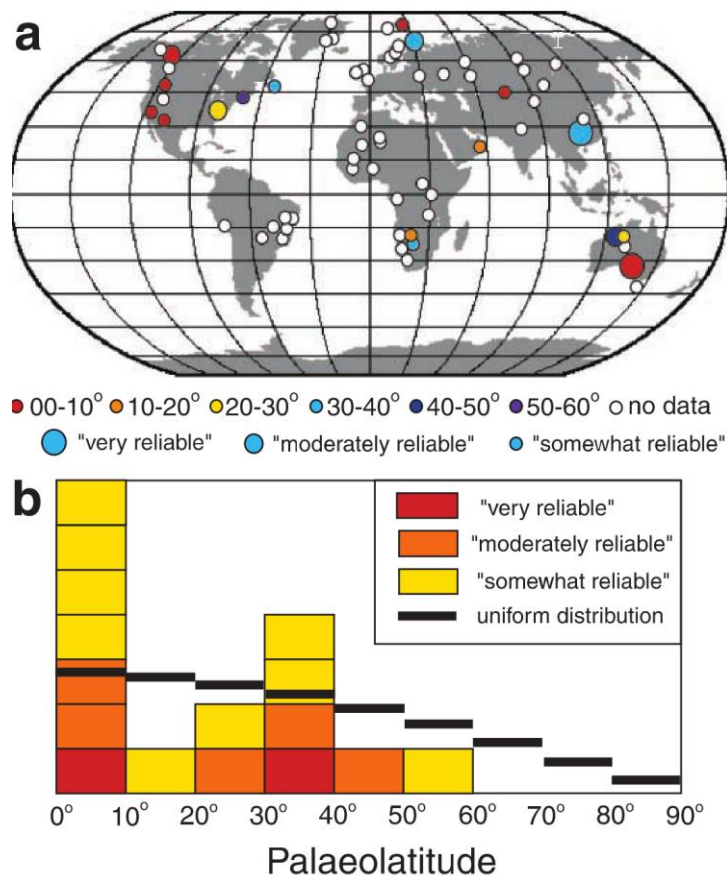


**Figure 7:** Showing the global distribution of LNGD with estimated paleolatitudes accompanied by a histogram showing the latitudinal distribution of LNGD. Source: (Schrag et al., 2002)

The carbon isotope record is another useful tool for understanding paleoclimate. We use the ratio of  $^{12}\text{C}$  to  $^{13}\text{C}$  as a proxy for the record of biogeochemical cycling, expressed as  $\delta^{13}\text{C}$ . The record, preserved through these carbon ratios, is one of anomalies occurring around LNGD deposits with generally elevated values prior to glaciation and lower values directly following glaciation (Hoffman and Schrag, 2002). While these general values are seen around all LNGD, in a number of locations, including the PAF on the Garvellachs a negative  $\delta^{13}\text{C}$  anomaly has been analysed prior to the glacial deposits themselves (Fairchild et al., 2017). These anomalies reflect the deposition of organic carbon and calcium carbonate from weathering. During the onset of glaciation an increase in the burial of organic matter leaves the residual carbon pool enriched. Following the glacial period organic burial is greatly reduced, thus depleting the ratio (Schrag et al., 2002). Occurring together with LNGD, these data are hard to dismiss; there was major disruption in the ocean and atmospheric systems occurring together with the deposition of glacial layers. While there remains debate over the interpretation of these data, their widespread supra-regional distribution is universally agreed upon (Hoffman and Schrag, 2002).

Banded iron formations (BIF) are found globally in association with LNGD. BIF occur as a fine-grained sedimentary rock with >15 wt % iron only commonly found in layers older than 1.85 Ga (Hoffman et al., 2017). A gap of more than a billion years in the global geological record occurs between the final BIF formation around 1.85 Ga and LNGD (Hoffman and Schrag, 2002). The distribution of BIF, in conjunction with glaciations and snowball related events, can be seen in figure 8. Hoffman et al. states that iron formation requires (i) anoxic water conditions in which Fe(II) can accumulate in solution; (ii) limited sulphur flux to prevent titration of dissolved iron as iron sulfide or, alternatively, insufficient organic material to support microbial sulfate reduction; and (iii) an oxidising agent to localise insoluble iron oxide production (Hoffman et al., 2017; Hoffman and Schrag, 2002).

The most interesting of these factors in this study, is the requirement of anoxic ocean conditions for iron to accumulate. The Paleoproterozoic occurrences seen prior to 1.85 Ga (figure 8) occur prior to the large excess of  $\text{O}_2$  accumulated in the atmosphere around 2.2 to 2.0 Ga and are synchronous with the  $\delta^{13}\text{C}$  excursion in marine carbonates (Karhu and Holland, 1996). This, together with Hoffman's statement that anoxic water conditions are required in order that formation can take place, it can be inferred that LNGD iron formations are facilitated by ocean anoxia. Ocean to atmosphere  $\text{O}_2$  exchange was inhibited due to stagnation beneath near-global sea-ice cover (Lowe et al., 1992). The anoxic conditions occurring in the oceans during a global glaciation allows for iron to accumulate in solution through generation at the mid-oceanic ridges or leaching from bottom sediments. As worldwide

glacial conditions changed, circulation was re-established allowing oxidation of the dissolved iron and formation of BIF in areas of oceanic upwelling (Hoffman et al., 2017).

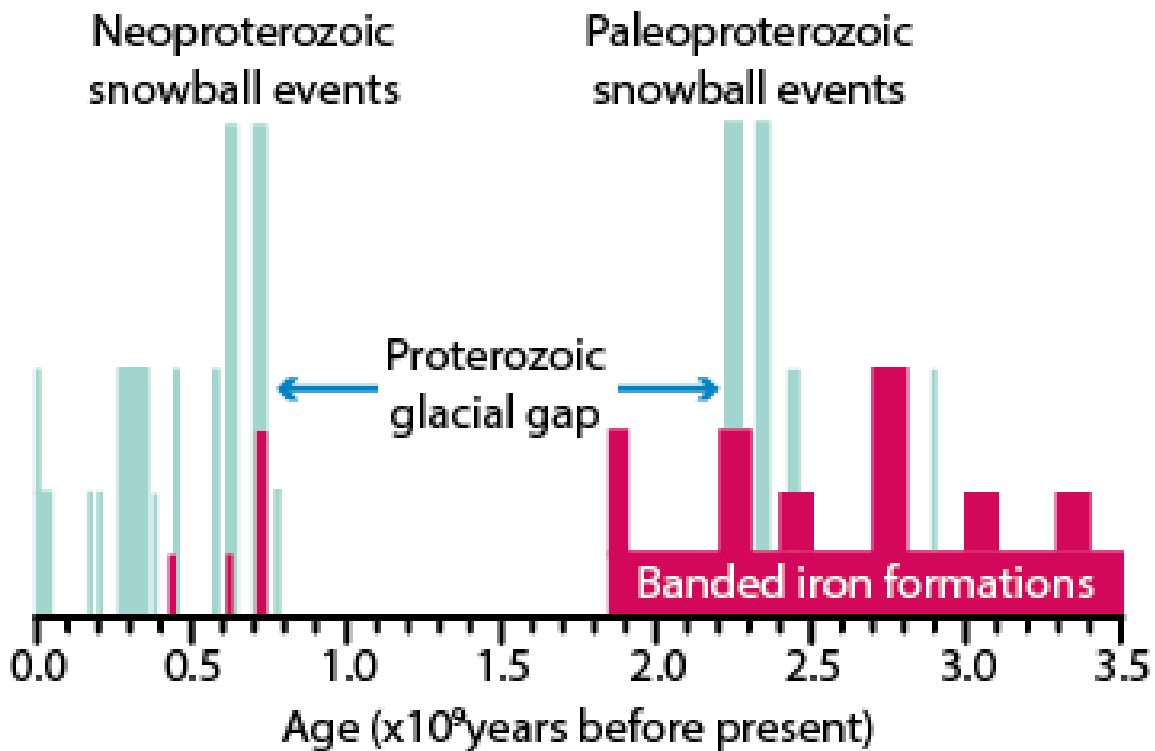


**Figure 8:** Retraced and adapted from Hoffman and Schrag, (2002) to show the temporal distribution of snowball events in pale blue against the occurrence of banded iron formations in red.

Cap carbonates represent another vital piece of evidence in terms of understanding Snowball Earth. Cap carbonates are laterally continuous units of lithologically distinctive carbonate overlying Cryogenian glacial deposits (Hoffman et al., 2017). These deposits have an extremely sharp basal contact without evidence of reworking or significant hiatus, suggesting deposition directly following the glacial termination (Hoffman and Schrag, 2002). Hoffman and Schrag also suggest deposition of cap carbonates generally extends beyond the glacial deposit itself. The carbonates cover preglacial rocks also, creating a disconformity at their contact. Further evidence linking these sequences of wide geographic distribution are a distinct and unusual set of sedimentary structures as discussed by (Hoffman and Schrag, 2002; James et al., 2001) as well as a consistent depletion in  $^{13}\text{C}$  relative to carbonate formations of a similar age (Hoffman et al., 2017). Consistent  $\delta^{13}\text{C}$  data for cap carbonates worldwide indicates depletion up-section, these values can be correlated for various global basins of the same period and are used as evidence for a secular change in seawater on a global level (Fairchild and Kennedy, 2007). These low  $\delta^{13}\text{C}$  values suggest a drastic reduction in biological productivity in the ocean (Hoffman, 1998).

Cap carbonates, primarily dolostone, appear throughout the geological record directly overlying glacial deposits, and as discussed, this suggests a remarkably quick shift from glacial to tropical conditions that occurred globally. This data fits the snowball model in terms of the extreme greenhouse conditions necessary for initiating deglaciation as well as the reverse effect of ice-albedo. High levels of CO<sub>2</sub> and increasing surface temperatures allow carbonic acid rain to precipitate onto a landscape rich in frost shattered surfaces and rock powder (from protracted glaciation) along with large volumes of unaltered volcanic material (Hoffman and Schrag, 2002). Further to this, Hoffman and Schrag state that exposed carbonate platforms led to primarily carbonate weathering, however, after a rise in sea level this switched to silicate weathering, helping to stabilise atmospheric CO<sub>2</sub> once more (Hoffman and Schrag, 2002). While the origin of cap carbonates is still a matter of debate, their link to glacial sequences is clear.

Despite the large amount of research, there remains several aspects of uncertainty with respect to the snowball hypothesis. Within LNGD deposits numerous deformation structures and striated clasts are found, these imply a warm-based glacial system which is incompatible with total snowball glaciation (Deynoux, 1985; Rice and Hofmann, 2018). It is important, however, to consider the chronology of events, if these striations were created during the recessive period of a snowball glaciation then we would still expect to see this type of structure. Some anomalous data is also detected within seawater isotope analysis conducted on cap carbonates overlying LNGD. The least altered <sup>87</sup>Sr/<sup>86</sup>Sr ratios analysed show little change from preglacial values. This suggests either an extremely short glaciation, incongruous with other evidence, or this ratio was buffered by carbonate dissolution (Hoffman, 1998; Hoffman and Schrag, 2002).

There is much discussion regarding the survival of certain species of eukaryotes during snowball events. While prokaryotic lifeforms, it is widely agreed, could survive such events, the record reveals a surprising number of eukaryotic species surviving through Neoproterozoic icehouse conditions. Some of these species may have been protected by refuges in brine channels of new sea ice or tidal cracks along ice-grounding lines, however, the overall rate of survival is at unexpected levels considering the intensity and duration of conditions suggested within this period (Hoffman and Schrag, 2002). Finally, computer models suggest that the necessary atmospheric CO<sub>2</sub> for deglaciation, is more than twice the generally accepted level (0.1 bar) (Pierrehumbert, 2005). Pierrehumbert (2005) goes on to state that data from his modelling found that even at these levels it was difficult to create a scenario in which the initiation of deglaciation was possible without adding yet unknown feedbacks into the formula. This is problematic, as, for a hard snowball to be considered, a realistic method of initiating deglaciation is needed, this model challenges the idea that greenhouse build-up catalysed/initiated the process of deglaciation.

There are several alternate theories to explain low latitude glaciation without using the snowball earth hypothesis. Slushball Earth suggests that while glaciation was indeed global, equatorial regions of the ocean remained open and unglaciated (Fairchild and Kennedy, 2007). Zipper-rift Earth links glaciations to rifting of the supercontinent Rodinia (Fairchild and Kennedy, 2007) and finally High-tilt Earth suggests that the Earth's obliquity during the Neoproterozoic allowed for glaciation of equatorial regions due to the distribution of solar energy being focused at the poles (Fairchild and Kennedy, 2007).

Key to this study are the glacial / interglacial layers of the Port Askaig Formation as well as other LNGDs. If we are to consider an increase in CO<sub>2</sub> concentration to be the most likely factor for initiating deglaciation of a Snowball Earth, then we expect to see a post-snowball world of greenhouse conditions as caused by the high atmospheric CO<sub>2</sub>. Contrary to this, as will be discussed in greater detail in section 2, within the PAF we see cyclic shifts back and forth between glacial and interglacial layers, giving us an archive of paleoclimatic shifts in out of icehouse conditions. This cyclic shift between glacial, interglacial and periglacial conditions recorded through deposition within the PAF can also be found throughout numerous other global LNGD (Evans, 2000). This provides one of the key stumbling blocks to the Snowball Earth hypothesis: if the route out of global glaciation and into warmer conditions is caused by very high atmospheric CO<sub>2</sub>, we should not expect then to see any interglacial periods in LNGD.

## 1.2 Review of Relevant Proxies.

Several climatological and environmental proxies will be used during this study in conjunction with data gathered during the field excursion. Each of these data sets will be studied in conjunction with one or more proxies to make an interpretation of palaeoclimatic and paleo environmental conditions in the Neoproterozoic. It is important to note, while interpreting data with established proxies, they remain just that, an interpretation based on the analysis of numerous datasets, caution should be used in terms of overreliance on proxies and data combining numerous proxies should be considered of greater scientific value.

Clift, et al., (2014) conducted a study of chemical weathering and physical erosion in conjunction with monsoon intensity in China 25 Ma. Chemical weathering causes changes to both bulk sediment chemistry and clay mineralogy. (Clift et al., 2014) uses the ratios of K/Al and K/Rb as a proxy since alkali elements are relatively mobile in water while aluminium and rubidium are less mobile during the breakdown of minerals, allowing us to analyse the remaining concentration of these elements to study chemical weathering of the source material, this is of use in this study. Through the analysis of

K/Rb particularly, this study will look at paleo fluctuations in chemical weathering, in which case lower values are expected to indicate more alteration of the source rock. Another important proxy for the study of paleoclimate is the Chemical Index of Alteration used within the study of Proterozoic climate by (Young, n.d., 1982). The ability of CIA analysis to indicate past chemical weathering conditions persists through low grade metamorphism of the material under analysis (Young, n.d., 1982). The dominant process during chemical weathering of the upper crust is the breakdown of feldspars leading to a shift in the ratio of alumina to alkali which can be analysed thus:

$$CIA = \left[ \frac{Al_2O_3}{Al_2O_3 + CaO + Na_2O + K_2O} \right] * 100 \quad (1)$$

Also discussed in (Clift et al., 2014) is the ratio of Ti/Ca as a proxy for processes of physical erosion. Ti, in this case, is dominated by the presence of heavy minerals such as ilmenite, perovskite, rutile and titanite while Ca is representative of biogenic carbonate.

Jakobsson et al., (2000) discuss in their research the use of manganese concentration as a proxy for deep ocean oxygenation. The presence of oxygen in ocean water in this case is considered to enable greater precipitation of manganese. When analysing Arctic sediments, it was considered thus, that an increase in manganese concentration represented periods of increased ventilation due to diminished sea ice. This suggests a possible link between manganese concentration and ocean waters being capped by ice providing us a proxy for sea ice cover to be used in conjunction with terrestrial proxies. Jakobsson et al., (2000) also notes that manganese concentration may fluctuate because of climate forcing of transport of material, for instance draining of peat areas, lake systems and boreal forests as this could deliver large quantities of manganese and create fluctuations in observed datasets. Due to the lack of vegetation during the Neoproterozoic, however, this should have no bearing on the data in this study. This proxy would be most appropriately used in conjunction with other proxies for glaciation.

## 2. GEOLOGICAL BACKGROUND OF PORT ASKAIG FORMATION

The bedrock of Islay is comprised of the Rhinns Complex, formed around 1800 Ma when Islay was a part of the supercontinent Columbia (Webster, et al, 2015). Following deposition of the Rhinns Complex there is a large gap in the geologic record known as the 'Boring Billion'. Following this geologic temporal gap, the Dalradian Supergroup was unconformably deposited whilst Islay was a part of the supercontinent, Rodinia, around 800 Ma (Webster, et al, 2015).

The Dalradian Supergroup itself is a dominantly siliclastic, metasedimentary succession (Prave et al., 2009): consisting of the Grampian, Appin and Argyll groups, deposited unconformably above the Rhinns Complex. This unconformity has been later affected by tectonic activity and is marked by shearing, known as the Kilchiaran Shear Zone. The Dalradian forms a NE-SW trending belt across Ireland and Scotland, as shown in figure 9 (Fairchild et al., 2017). The Grampian group consists of the Colonsay and Bowmore groups, which were deposited into faulted basins. Subsequently, the Appin and Argyll groups were deposited as continental shelf sediments, first in a marine gulf and later in the open ocean. The Appin Group consists of the Maol an Fhithich Quartzite, Glen Egedale Phyllite, Kintra Dolostone, Ballygrant and the Lossit Limestone. The Argyll Group, on Islay consists of the Port Askaig Formation, Bonahaven Dolomite, Jura Quartzite and the Easdale and Crinan Subgroups (Webster, D.; Anderton, R.; Skelton, 2015). Two key geologic events that affected these depositional sequences are, the initial rifting of Rodinia around 840 Ma and the opening of the Iapetus shortly after 600 Ma, causing a shift in depositional environment (Webster, et al, 2015).

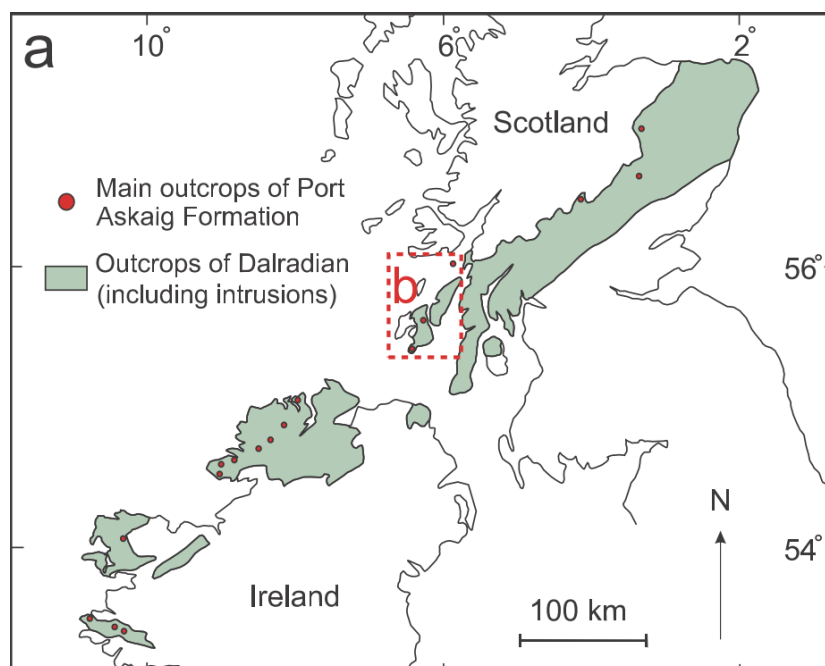


**Figure 9:** Illustrating the distribution of the Dalradian with the red dots marking the outcrops of the Port Askaig Formation itself. Source: (Fairchild et al., 2017)

Directly underlying the Port Askaig Formation is the Lossit Limestone. The Lossit Limestone on Islay consists of interbedded dolostone, quartzite, slate and mixed lithologies overlying 70 m of pure limestone, which in turn overlies several thick slate and limestone units (Arnaud, E., et al., 2011). The Lossit Limestone also contains oolites, formed in shallow waters under high energy current conditions along with occasional stromatolites, providing further evidence of the warm, shallow depositional environment (Arnaud, E., 2015; Webster, D., 2015)

Directly above the Port Askaig Formation is the Bonahaven Dolomite Formation, this dolomite is a 'cap carbonate' (discussed in section 1.1) and is believed to be the result of a dramatic climatic shift directly following the hypothesised snowball earth sequence. Illustrating this shift in climate, the dolomite sections contain rippled sands, mud cracks, and some dramatic stromatolite mounds as depicted in figure 10 (Arnaud, E., 2015; Webster, D., 2015). Together these features suggest deposition in warm, shallow, marine environments.



**Figure 10:** Stromatolite bioherms outcropping on the north shore of Islay, stromatolites outlined in red.

The Bonahaven Dolomite Formation itself consists of four members, from the basal sandstones containing dolomitic sandstones moving up sequence to thickly bedded sandstones. Before transitioning to stromatolite bearing dolostone and finally sandstone with large white dolomite formations (Spencer and Spencer, 1972).

The Port Askaig Formation (PAF) is a stratigraphic unit occurring near the middle of the Dalradian Supergroup (Ali et al., 2017). The Port Askaig Formation (PAF) itself comprises a fantastic archive of climatically related depositional episodes (Ali et al., 2018). The PAF can be seen in outcrop in at least 30 localities from Ireland to NE Scotland. It generally occurs in 100 m to 500 m intervals but can be seen in its most complete form around Port Askaig and the Garvellachs (Ali et al., 2017). This archive,

as referred to by Ali et al. (2018), is made up of 28 glacial, 25 periglacial and 23 non-glacial units (Ali et al., 2017; Kilburn et al., 1965; Spencer, 1971); consisting of a succession of diamictite interbedded with sandstone, conglomerate and mudstone (Arnaud and Eyles, 2006). These stratigraphic units, are correlated with the Sturtian glaciation 717 Ma – 659 Ma (Benn and Prave, 2006; Hoffman et al., 2017; Rooney et al., 2015). Current best estimates suggest 30°S as the palaeolatitude of deposition for the PAF while it was located on the supercontinent of Rodinia (Benn and Prave, 2006).

Following deposition, a major influence on this formation was the Grampian Orogeny, which formed the Grampian Mountains, occurring at around 470 Ma (Chew and Strachan, 2014). This event caused significant folding throughout the Islay stratigraphy as well as the formation of the Islay anticline.

The diamictite beds of the formation are split up into members 1 – 3 on the Garvellachs and 4 – 5 on Islay (Ali et al., 2017). The lithological composition of the diamictite matrix changes up sequence. Ali et al. (2017) states that member 1 is composed of dolomitic siltstones, including the distinctive sedimentary units of the Great Breccia and Disrupted Beds (Arnaud and Eyles, 2002). Member 2 changes from sand-rich dolomitic siltstones to dolomitic, silty arenites. Finally, in members 3 and 4 silty arenites can be observed (Ali et al., 2017).

Ali et al. (2017) also discusses clast lithology and identifies throughout the sequence; dolomite, limestone, intrabasinal unknown, granite, quartzite, extrabasinal unknown and unknown clasts. Overall, throughout the sequence, an upward change occurs in clast lithology which can be expressed as the ratio of dolomite to granite stones (Ali et al., 2017). However, member 1 contains only intrabasinal clasts. Extrabasinal clasts first become prominent towards the top of member 2. No intrabasinal clasts can be seen at the top of Member 4 (Ali et al., 2017). Through member 5 there continues the trend throughout the sequence of upward lithological change from dolomitic to granitic lithology.

Diamictite 13, contained within member 1, is the most distinctive and unusual layer within this sequence, it is called the Great Breccia. The Great Breccia is over 50 m thick and consists of dislocated and folded rafts of dolostone, siltstone and sandstone (Benn and Prave, 2006). This is a matrix-supported diamictite containing large clasts up to hundreds of metres across (Arnaud and Eyles, 2002), this makes the Great Breccia particularly distinctive, the largest clasts elsewhere in the sequence are around 1 m across. Some of the larger clasts within this unit also exhibit both brittle and ductile deformation of their internal structure (Arnaud and Eyles, 2002).

Both Kilburn et al. (1965) and Spencer (1971) identified the Great Breccia as a till, Spencer in 1971 noting it's analogous nature to the Cromer Till occurring in the north of Norfolk, England (Benn and

Prave, 2006; Kilburn et al., 1965; Spencer, 1971). While its glacial origin has remained a primary avenue of interpretation for this diamictite, it has also been interpreted by Arnaud and Eyles (2002) as the product of subaqueous sediment gravity flow processes (Arnaud and Eyles, 2002). This is a very different origin theory to the more traditional glacial interpretation, it does, however, agree with some interpretations of tectonically active conditions in the basin at the point of deposition, as made by Schermerhorn and Eyles (Arnaud and Eyles, 2002; Schermerhorn, 1974).

Another distinctive unit within the PAF is the Disrupted Beds, a very heterogeneous group of rocks which exhibit large vertical and lateral variability (Kilburn et al., 1965; Spencer, 1971). They have a distinct banded appearance, consisting of alternating layers of cream-coloured dolostone, laminated dark-blue siltstones which are likely iron formations and diamictite (Benn and Prave, 2006). The interpretation of the Disrupted Beds is, again, divisive. Some researchers have noted the features they share with subglacial glaciectonites and tills, and have therefore surmised that the beds are a record of deformation by grounded ice, representing proglacial and subglacial components (Benn and Prave, 2006). An alternative theory, as with the Great Breccia, is that the beds record subaqueous slope failures (Arnaud and Eyles, 2002).

The Port Askaig Formation, in terms of this study is of particular use due to its 'stratigraphic completeness' as indicated by gradual, progressive changes in lithology, repeated patterns of environmental change in top and basal contacts, the high number of discrete climatically related episodes and that these are the thickest exposures of Neoproterozoic successions available for study (Ali et al., 2017).

The PAF, as mentioned above, consists of alternating layers of glacial and interglacial deposits, reflecting drastic paleoclimatic shifts that challenge the Snowball Earth hypothesis (Ali et al., 2017; Kilburn et al., 1965; Spencer, 1971). Through this evidence we can define some cyclicity in the climatic cycles reflected through these depositions. Another key feature in this formation that helps us identify cyclicity is the presence of evidence indicating permafrost surfaces. Features such as ice wedge polygons and frost shattered clasts indicate periglacial conditions during the shift between cold and warm climatic conditions (Ali et al., 2017). The PAF contains diamictite layers containing far travelled clasts within its matrix, the interglacial sandstone, mudstone and dolomite layers have no such clasts, highlighting further the shift in conditions between these repeated layers and the cyclicity found throughout the unit. There are 26 horizons including periglacial features in the formation, these are surrounded by 28 glacial episodes and 23 non glacial episodes meaning within 1100 m there occur 76 discrete climatically-related cyclic episodes (Ali et al., 2017).

### 3. METHODS

#### 3.1 Sedimentary log

A sedimentary log of the upper parts of the Port Askaig Formation (located on the eastern shore of Islay) was constructed between Port Askaig (55°50'54.98"N, 6° 6'23.02"W) and Port Bhoraraic (55°49'0.29"N, 6° 6'18.63"W) along a 4 km stretch of the sequence shown in figure 1. A short stretch directly south of Port Askaig, approximately 270 m, was not logged during this excursion. This short area was judged not to be safely accessible for the purposes of this study.

All occurrences of diamictites were logged, along with approximate layer thicknesses. Sedimentary layers that could be identified were also logged and measured. Dip direction and the angle of the beds were recorded where possible. A record was also made of each fault, potential fault or intrusion found throughout the sequence. Any indication of fossilised permafrost surfaces was also recorded within the log, including ice wedge polygons and ice shattered clast surfaces. Data was collected over 3 days in the field. The stretch from Eas Forsa to Fhion Phort (as seen in figure 1) was logged alone, whilst the remaining log was made with Maria Strand in conjunction with her thesis project.

#### 3.2 Handheld XRF method

XRF measures solid samples using X-ray irradiation, causing the expulsion of a core shell electron. When the electron is displaced, the rest of the atom compensates for this shift, by rearrangement of electrons from outer shells. The energy release as the outer shell electron falls to a lower energy level is emitted as a photon, generating a detectable and analysable fluorescence. The wavelength of the emitted fluorescence provides a unique signature that can be compared to samples of known elements. The elemental composition of the sample surfaces can therefore be identified both qualitatively and quantitatively. Detection limits of XRF are as low as parts per million (ppm) in rock samples, further information on the specifications of the device can be found in the user manual (User Manual Delta, 2010)

XRF measurements (made using a Delta Professional Handheld XRF Analyser, Olympus) were taken along a 7 m length of a single sandstone layer outcropping at a roadcut at Port Askaig (55°50'54.98"N, 6° 6'23.02"W). Each layer was analysed, moving across the outcrop to preserve continuity as necessary. The line of analyses across the outcrop was selected to analyse as many sequential layers as possible. Analyses were initially taken at 1 cm increments, however, due to the time limitations, 2 cm increments were chosen to cover the remainder of the layer.

The chemical composition data were analysed using OriginPro 2017. Fluctuations in manganese content throughout the sample were used as a proxy for ocean bottom oxygenation as discussed by

Jakobsson et al. (2000). The ratio of potassium to rubidium was used as a proxy for chemical weathering as discussed by Clift et al. (2014). Data for silicon, potassium, and calcium have also been included as these are good indicators for quartz, mica and carbonate content. Each of these results, except for K/Rb have been adjusted for light elements. Portable XRF suffers from the restriction of light elements. Light elements are defined as elements with an atomic number of 11 or lower, for some their fluorescence is unable to escape the surface without being absorbed, others will be unable to penetrate the air. Both scenarios make detection impossible. Due to air and vegetation occurring between the detection window and the sample and comprising light elements I have adjusted my results for manganese, silicon, potassium and calcium to compensate for this. The method used for this was, for instance, in the case of manganese:

$$\mathbf{Mn} = Mn (measured) * \left( \frac{100}{100-LE} \right) \quad (2)$$

This result allows for more accuracy in terms of the sample itself. Uncertainty was calculated for the ratios using error propagation. As the instrument provided error values for both results in the ratio it was necessary to calculate a combined value for uncertainty. This was done as follows, for a ratio of x over y where  $\delta x$  is the uncertainty for x and  $\delta y$  is the uncertainty for y:

$$|\text{Ratio}| \cdot \left[ \left( \frac{\delta x}{x} \right)^2 + \left( \frac{\delta y}{y} \right)^2 \right]^{1/2} \quad (3)$$

## 4. RESULTS

### 4.1 Sedimentary log

The sedimentary log taken of the Port Askaig Formation is shown in Figure 12. The log begins at Port Askaig (55°50'54.98"N, 6° 6'23.02"W) and covers an area of around 4 km, ending at Port Bhoraraic (55°49'0.29"N, 6° 6'18.63"W).

10 discrete outcrops of diamictite (examples shown in figure 11) were logged, each are separated in the sequence by sedimentary deposits that were identified in the field. This entire sequence has been metamorphosed at greenschist facies conditions (Prave et al., 2009), as such all sedimentary deposits are metasedimentary. For clarity in this log, however, metasedimentary deposits will be referred to without the 'meta', for instance, 'sandstone' as opposed to 'metasandstone'. At Port Askaig, sandstone was identified, highly arenitic sandstone was also found in the most northern section of mapping carried out. Both mudstone and sandstone were found in the middle part of the logged area with two deposits of each. On both occasions the two sedimentary deposits of the same type are interrupted by faulting. In the most southern area mapped numerous deposits of highly arenitic sandstone are shown, this area of the study represents the last of the PAF prior to encountering the Jura Quartzite. Finally, a single outcrop of dolostone was found following the final arenitic sandstone mapped.

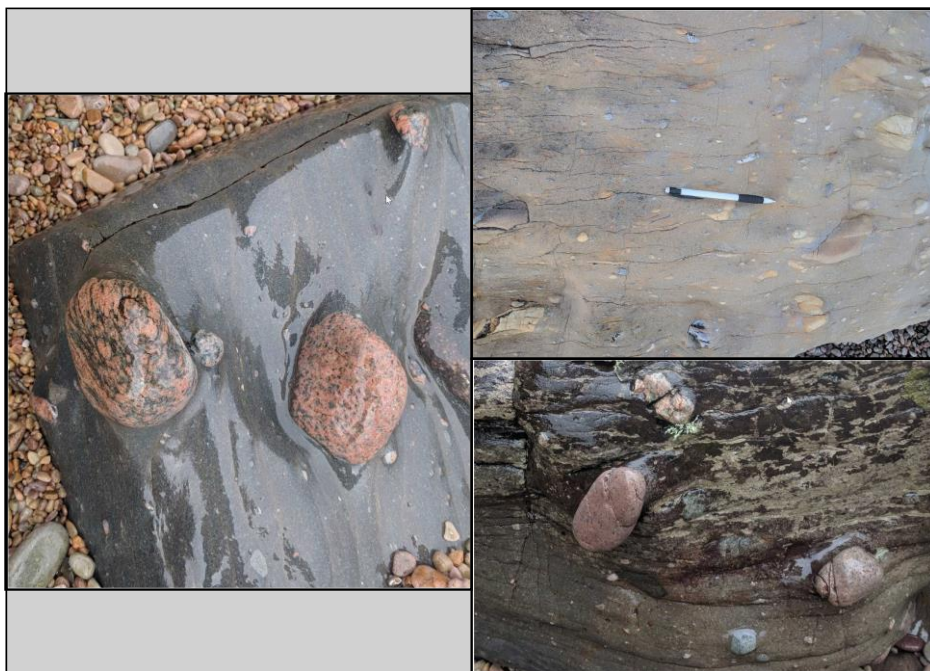


**Figure 11:** Examples of diamictite as observed in the field.



Figure 12: Sedimentary log of Port Askaig Formation showing glacial / interglacial layers between 55°50'54.98"N, 6° 6'23.02"W and 55°49'0.29"N, 6° 6'18.63"W.

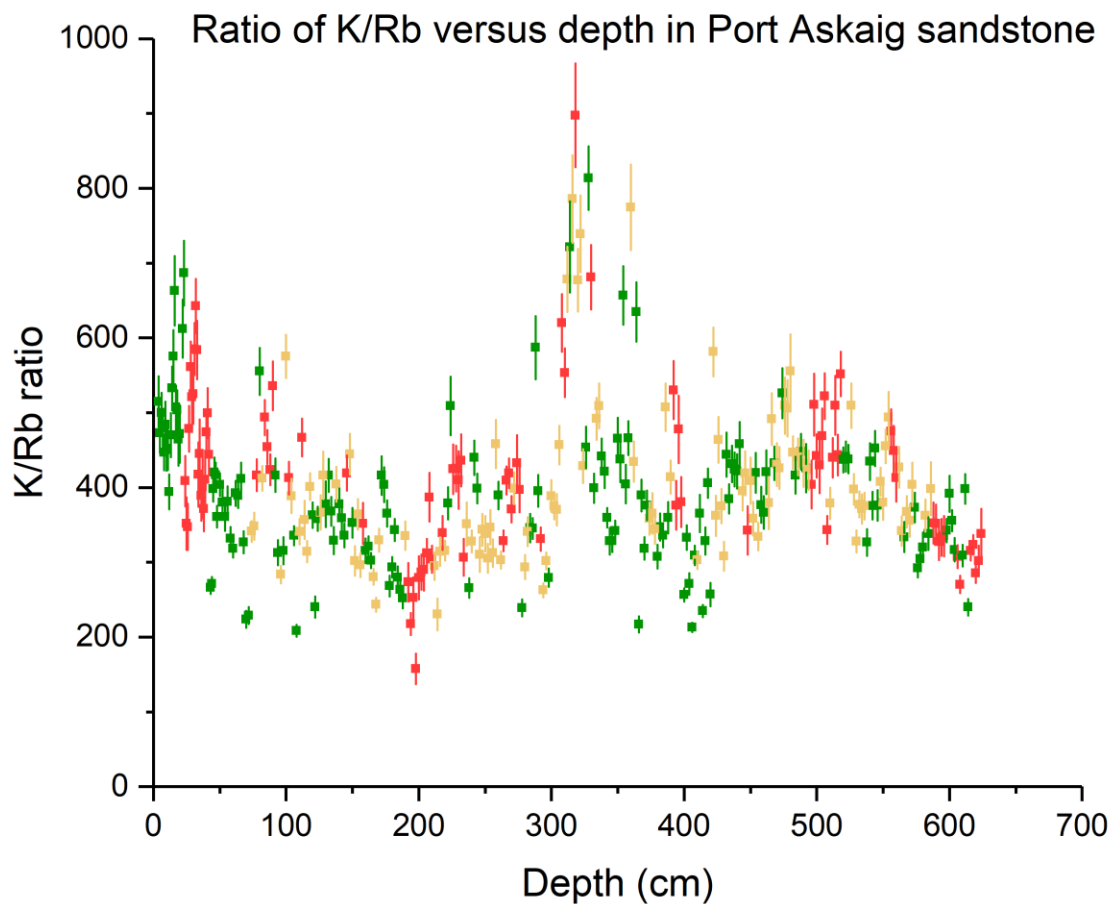
There were numerous areas of no exposure found in the coastal section, several of these displayed the erosive and vegetative characteristics of sedimentary deposits. As such, we would expect there to be a number more distinct diamictites and sedimentary deposits not identified in this study but occurring in the stratigraphy.

A total of six faults are shown in the log, these were each identified in the field and we see some repetition of layers surrounding the faults, this is particularly noticeable at points A and B indicated on the log. Dykes were also logged when found in the field, the majority occurring within diamictite layers.

Observation was also made of several periglacial indicators within the studied area of the PAF. At one location evidence of ice wedge polygons was noted and at two different locations possible frost-shattered clasts were observed. These are shown in figure 12.

## 4.2 Handheld XRF data

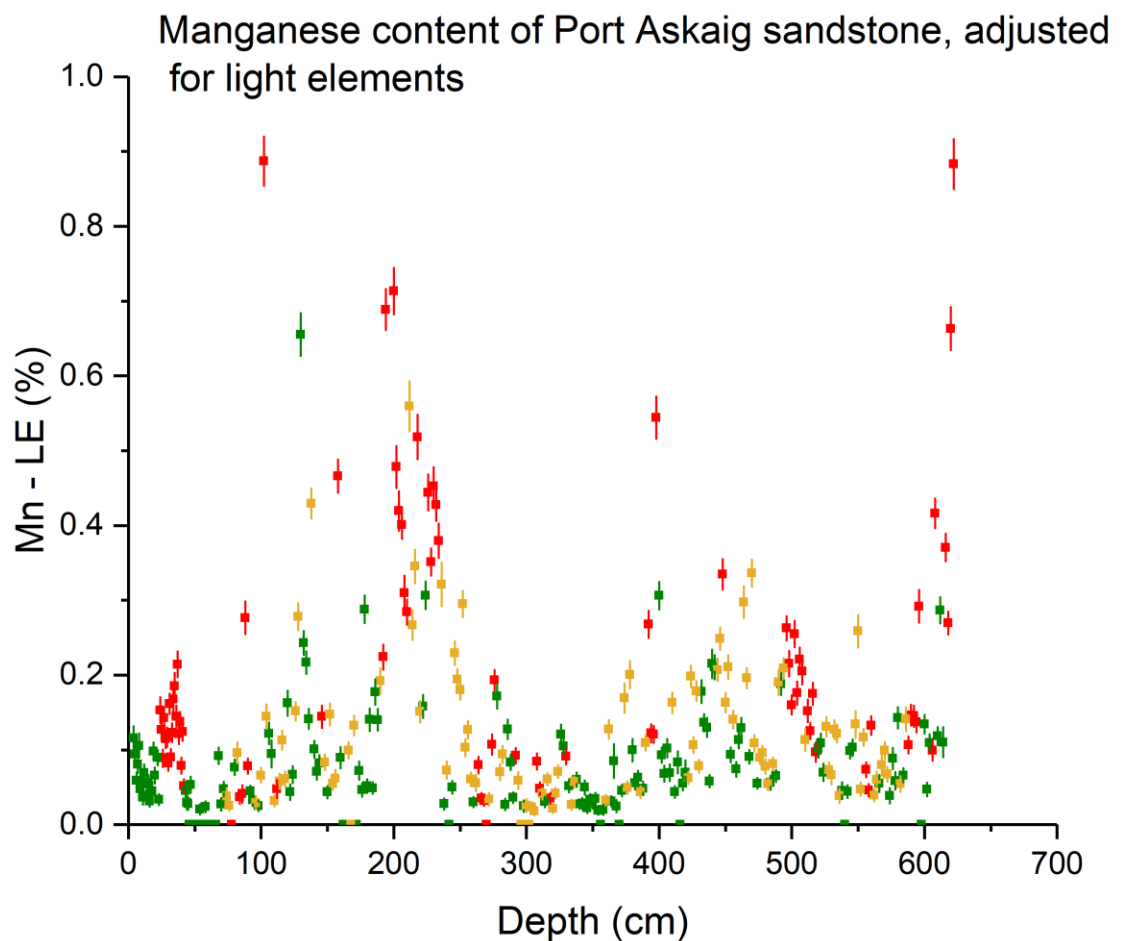
Figure 13 shows the ratio between potassium and rubidium plotted against depth within the sandstone layer analysed at Port Askaig. Cyclicity is clearly shown in these results, with noticeable highs at 25 cm and 325 cm while distinct lows in the data occur at 200 cm, 400 cm and 600 cm. The cyclic changes are most clearly defined in the red layers, still quite well defined in the red/green and noticeable but less correlative in the green layers.



**Figure 13:** Ratio of potassium to rubidium plotted against depth for sandstone outcrop near Port Askaig. The colours correspond to the colours of the layers in the outcrop with yellow representing layers between red and green.

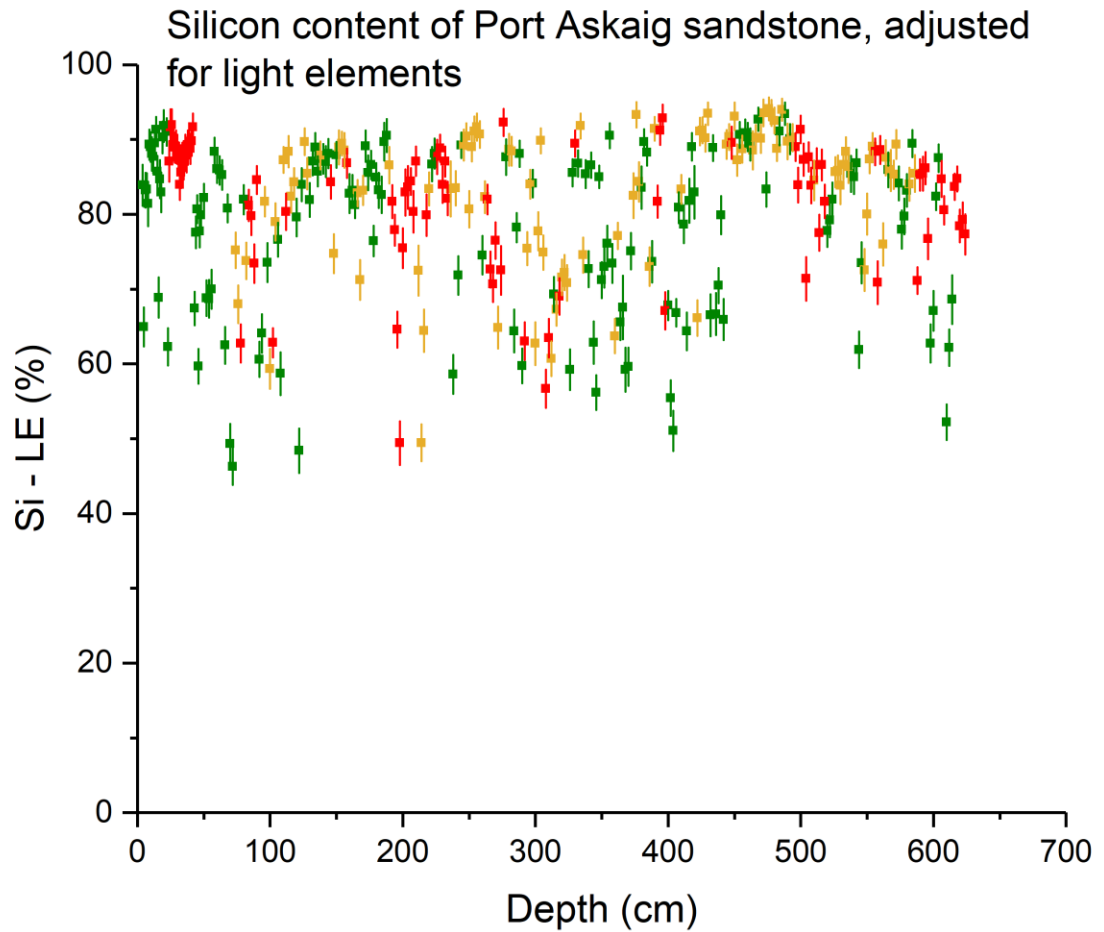
For each of the single element analyses, light elements were removed using equation 2. This means that the plotted values relate to the percentage of the metallic (and silicon) content of each analysis.

Figure 14 shows the manganese content plotted against depth within the sandstone layer analysed at Port Askaig, adjusted for light elements. There is a similar trend, highs occurring within the data at around 200 cm, 450 cm and 600 cm. Again, the most distinct correlation is in the red layers, a less noticeable trend in red/green and the least noticeable but still interesting variation shown in the green layering of the sandstone.



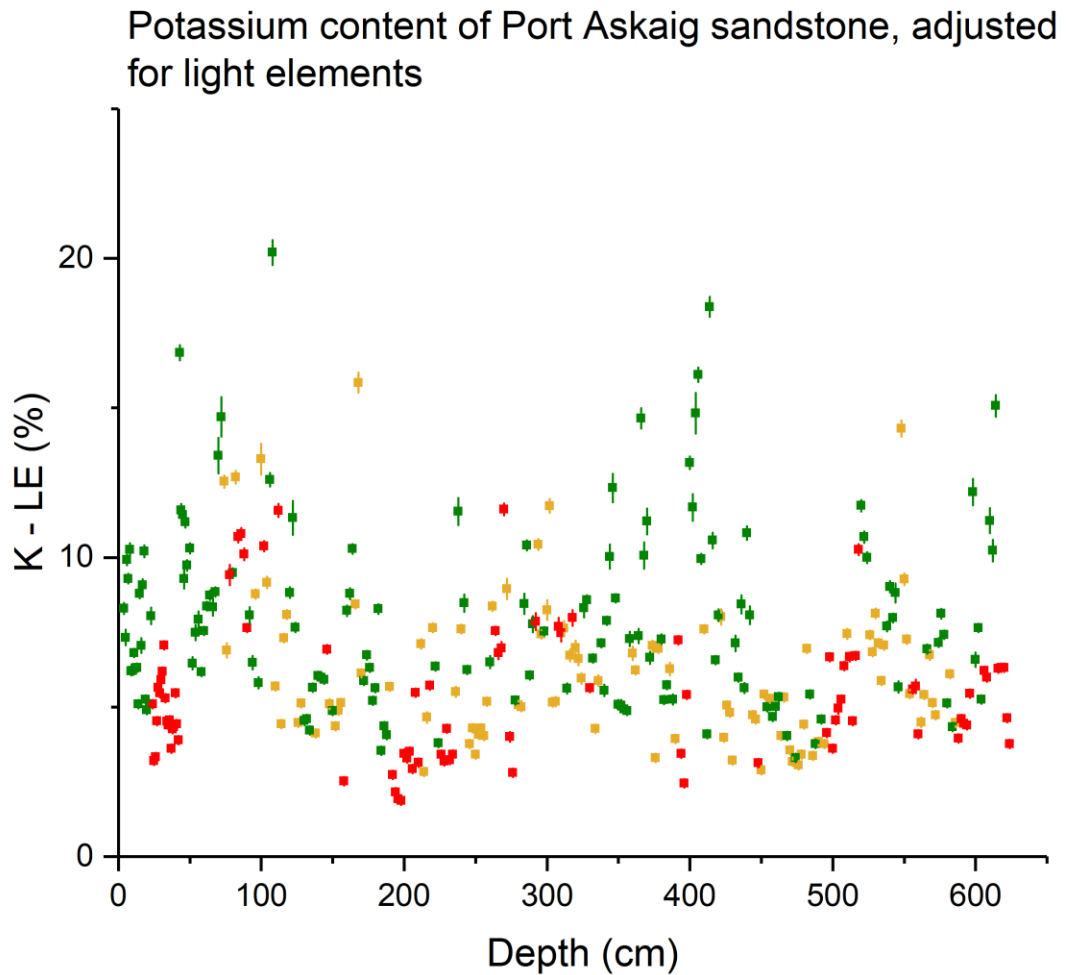
**Figure 14:** Manganese content adjusted for light elements plotted against depth for sandstone outcrop near Port Askaig. The colours correspond to the colours of the layers in the outcrop with yellow representing layers in between red and green.

Figure 15 shows the silicon content for the sandstone at Port Askaig as plotted against depth, adjusted for light elements. There is not a huge amount of correlation on this graph, as the sample is of a sandstone we see quite high and consistent levels of silicon.



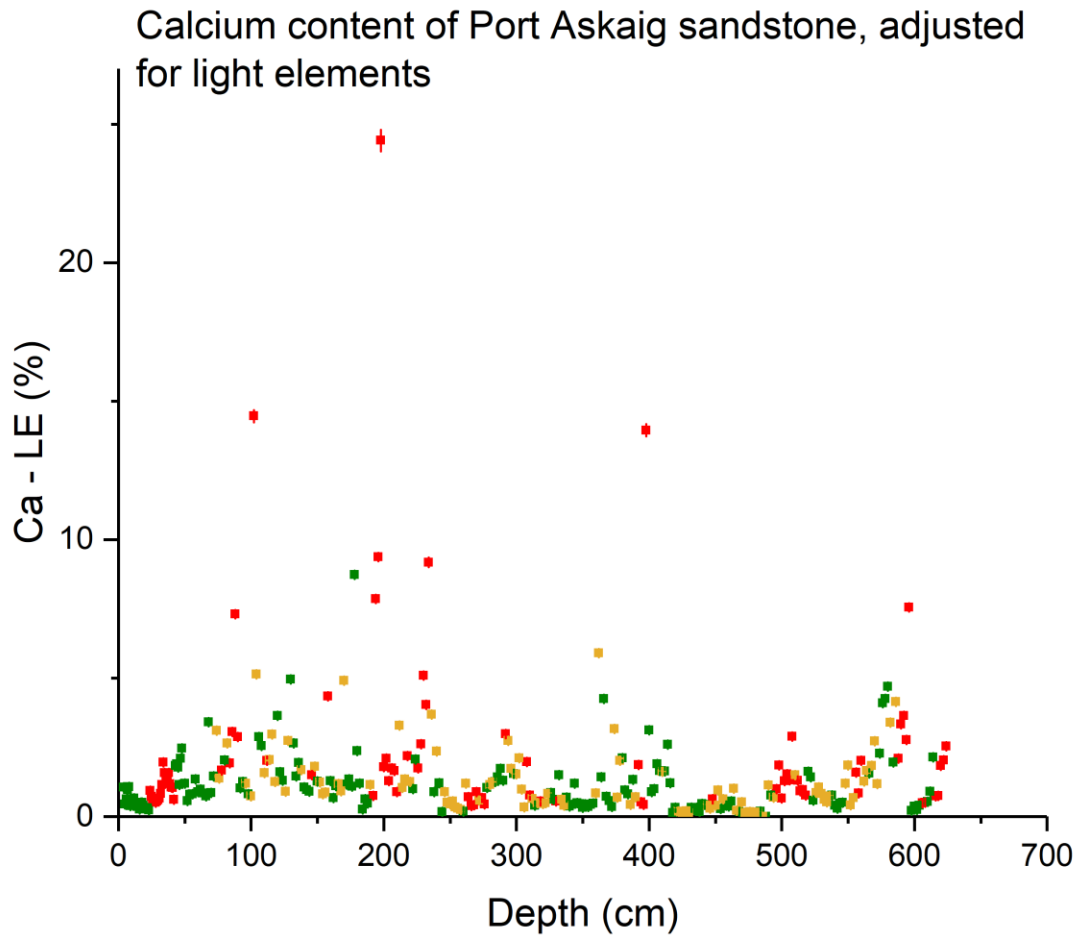
**Figure 15:** Silicon content adjusted for light elements plotted against depth for sandstone outcrop near Port Askaig. The colours correspond to the colours of the layers in the outcrop with yellow representing layers between red and green.

Figure 16 shows the potassium content of the sandstone at Port Askaig plotted against depth, adjusted for light elements. This graph shows a widely distributed cyclicity across the depth of the layer. The most pronounced trend is exhibited here throughout the green layers, less so in the green/red layers and least so in the red layers.



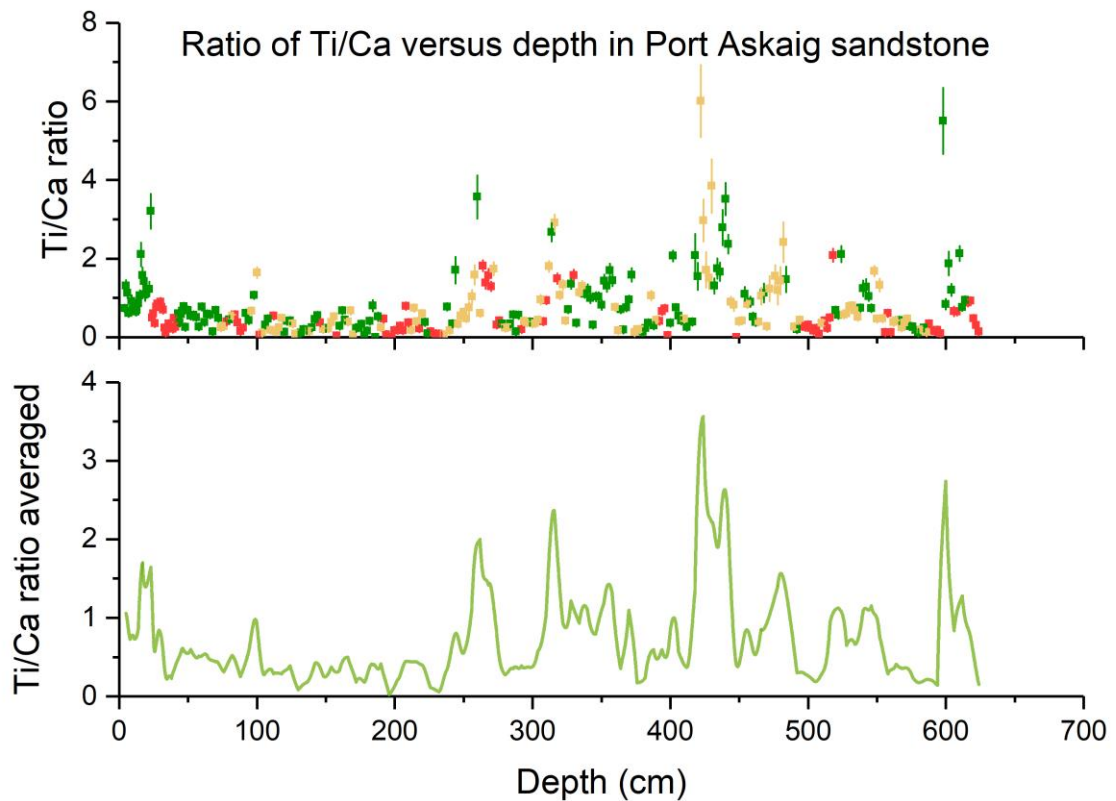
**Figure 16:** Potassium content adjusted for light elements plotted against depth for sandstone outcrop near Port Askaig. The colours correspond to the colours of the layers in the outcrop with yellow representing layers in between red and green.

Figure 17 shows the calcium content of the sandstone at Port Askaig, plotted against depth and adjusted for light elements. This data displays some minor cycles with a similar distribution throughout the differing coloured layers. There are some outlying red data points of far higher value shown within this data.



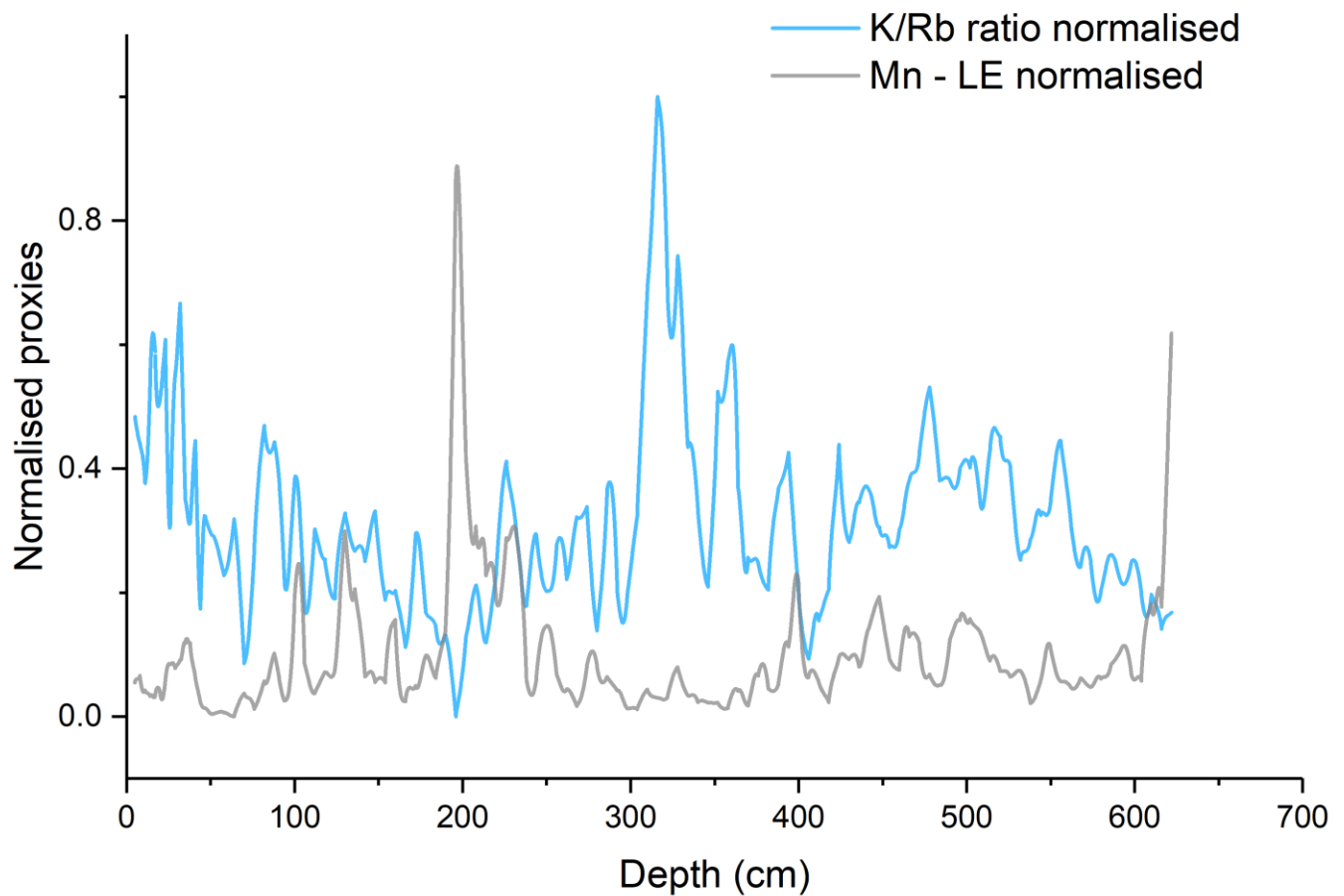
**Figure 17:** Calcium content adjusted for light elements plotted against depth for sandstone outcrop near Port Askaig. The colours correspond to the colours of the layers in the outcrop with yellow representing layers in between red and green.

Figure 18 shows the plot of Ti/Ca, used as a proxy for physical erosion by (Clift et al., 2014), also presented is a line graph showing the average of each three data points. From this we can see a number of distinct increases in the ratio value around 250 cm, 300 cm, 420 cm and 600 cm.



**Figure 18:** Ratio of titanium to calcium plotted against depth for sandstone outcrop near Port Askaig. The colours correspond to the colours of the layers in the outcrop with yellow representing layers in between red and green. Panel two provides an average of each three data points plotted to a line for a clearer picture.

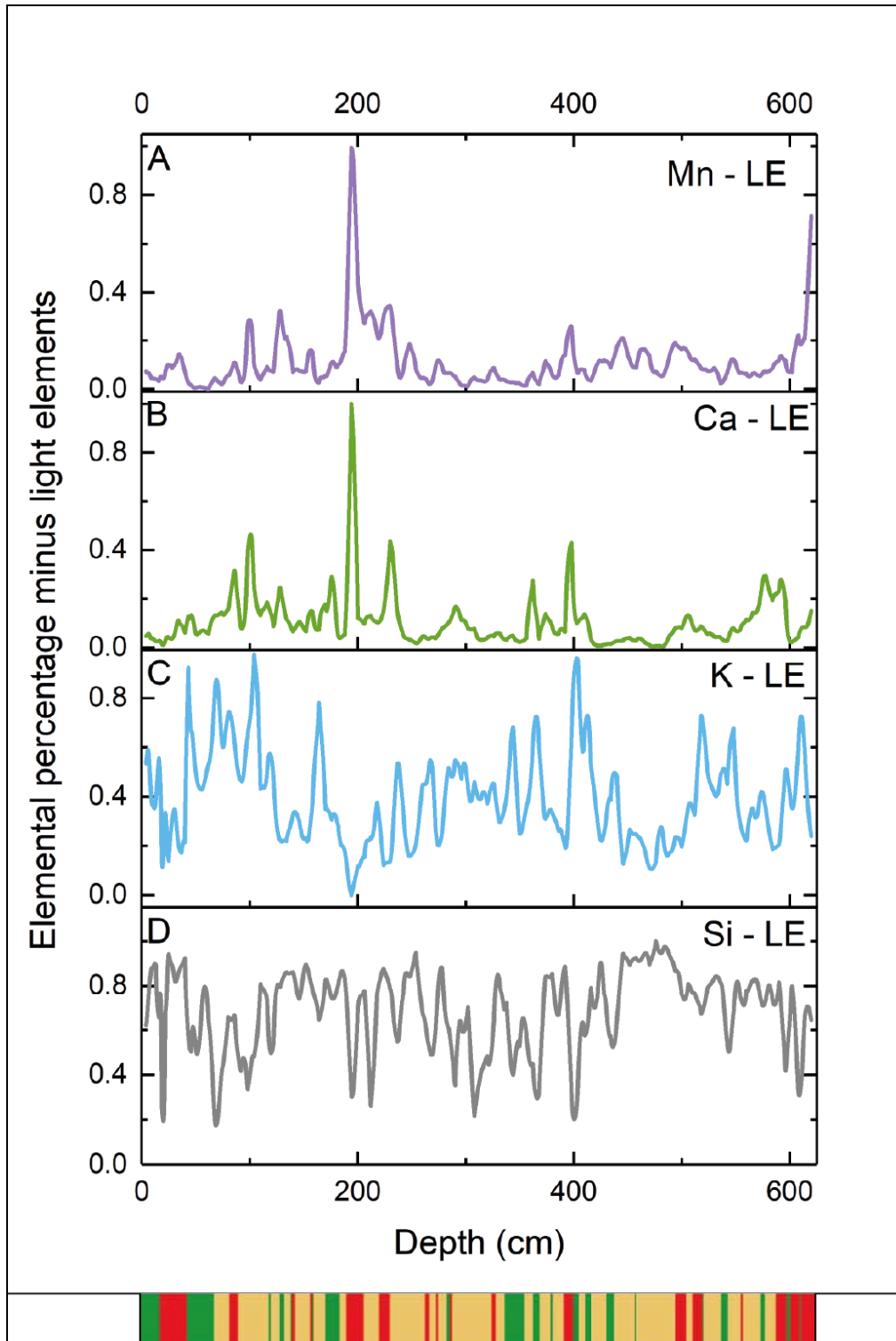
Figure 19 shows a comparison between manganese minus light elements and the ratio of potassium to rubidium, these have been normalised to be overlain and provide a comparative perspective on the data. The ratio of potassium to rubidium shows one large and distinctive peak which occurs concurrently with relatively low values of manganese. There are also several distinct dips in the K/Rb ratio value, occurring around 200 cm and 600 cm, these are each matched by noticeable increases in the values for manganese over a similar period.



**Figure 19:** Showing normalised values of K/Rb ratio and Mn. Each have been calculated to remove light elements and an average taken of each three data points to smooth the dataset.

Figure 20 presents a comparison between several useful elements across then depth of the analysed sandstone. Manganese and calcium show some strong similarity in their distribution, with a particularly significant peak around the 200 cm mark. These two also show some concurrent shifts throughout the rest of the analysed area. Potassium moves mostly independently of the first two elements however around the large peak at 200 cm for calcium and manganese we do see a pronounced dip in the value for potassium. In panel D, the values for silicon are plotted and these

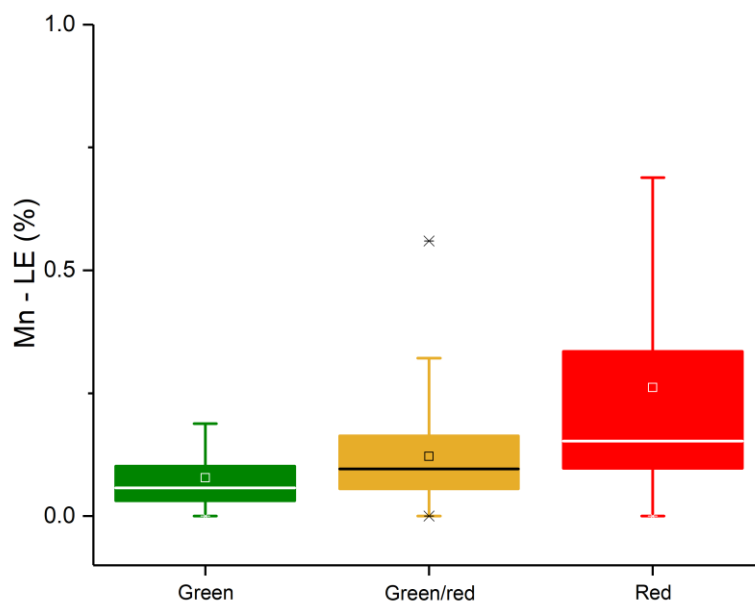
seem to move mostly independently of other elements, except that there are large dips in its values around 200, 400 and 600 cm. It is worth noting, however, that these dips in the value of silicon are not unique but are repeated throughout the sample, unlike the excursions noted in other elemental datasets.



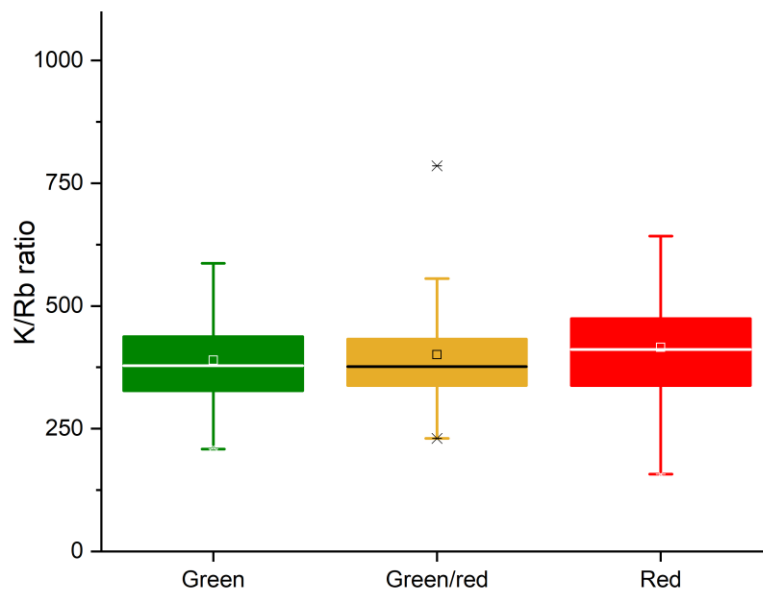
**Figure 20:** Showing the total elemental percentage across depth of Si, K, Mn and Ca. Each have been calculated to remove light elements and an average taken of each three data points to smooth the dataset. Also shown is a profile of the colour of the sandstone at the point of detection as observed in the field.

Figure 20 shows normalised versions of both Mn – LE and K/Rb ratio, this was achieved by finding the average of each three data points in the dataset. The resulting data were then plotted against each other as a line graph in order to show the comparison between the two proxies in question.

Figures 21 and 22 have utilised box plots to further analyse the comparison between the observable cyclicity of the red and green layers displayed in the sandstone and the variations in elemental concentration throughout the sample. For the K/Rb plot we see little correlation, in this case there appears to be little or no link between the variations in potassium and rubidium and the shifts in colour throughout initial deposition. In contrast, the data in figure 21 displays a notable correlation between the two, with far greater extremes and variability in the red layers than there are in green, in addition the green/red layers have intermediate variability and values between the two.



**Figure 21:** Box plot comparing the colour of depositional layers observed in the sandstone to the concentration of manganese throughout the sample.



**Figure 22:** Box plot comparing the colour of depositional layers observed in the sandstone to the ratio of potassium to rubidium throughout the sample.

### 4.3 Further Analysis

The analysis shown in figures 13 – 22 represents a spectrum of available proxy data, an attempt was also made to calculate the CIA however  $\text{Na}_2\text{O}$  is outside the detection limit of the handheld XRF device, categorised instead with light elements. In addition, many of the measurements in this study have no aluminium detected. As such, the remaining formula is insufficient to offer significant data, leaving K/Rb or K/Al as the most useful indicators of chemical weathering available. Due to the lack of aluminium in many of the analyses in this dataset, however, K/Rb thus becomes the most reliable data for paleo changes in chemical weathering available.

## 5. DISCUSSION

### 5.1 Sedimentary log

The sedimentary log illustrates at least 9 distinct beds of diamictite and 10 different sedimentary beds. Two of these sedimentary beds are repeated by faulting while the final contact noted is between dolostone and quartzite. In summary, this log represents, based on the glacial interpretation of the PAF (Ali et al., 2017; Kilburn et al., 1965; Spencer, 1971), likely around 7 shifts between glacial and interglacial climatic conditions interspersed with evidence of periglacial conditions.

This study is based on the upper parts of the PAF, located within the latter stages of the archive, following the distinctive Great Breccia and Disrupted Beds sequences. Critically, this represents an uncertain period in terms of our understanding of the Snowball sequences. We see here shifting back and forth between glacial and interglacial beds as shown in the log in figure 12. The most likely explanation for the marked cyclic climatic shifting that we find here is the impact of orbital forcing driven by Milankovitch cycles during the warming period directly following snowball glaciation.

This sedimentary log largely concurs with the literature on the topic (Ali et al., 2017; Kilburn et al., 1965; Spencer, 1971), suggesting a series of alternating glacial and interglacial layers formed of diamictite and metasedimentary deposits.

## 5.2 Handheld XRF data

The sandstone in question was deposited in shallow equatorial seas between 717 Ma and 659 Ma (Hoffman et al., 2017; Webster, D., et al, 2015). The literature and the sedimentary log (Figure 12) (conducted on Islay's east coast during this study) indicate that the deposition of this unit occurred between two distinct layers of, most likely, glacial deposition.

Figure 14 shows the ratio of potassium to rubidium plotted against depth throughout the sandstone outcrop. The colours used for the data points represent the colours of the sandstone at the point of each analysis. The distinctive shifts in colour of this sandstone between red, green and a combination of the two highlights distinct depositional cycles occurring throughout the deposition of this sedimentary rock. Figures 21 and 22 illustrate the link between colour shifts within the sandstone and the chemical analyses conducted in this study. From figure 22 we see little to no correlation, suggesting that the shifts in K/Rb, used as a proxy for chemical weathering are uncoupled from the depositional cycles reflected by the shifting colours of the red/green layering. In contrast to this, figure 21 shows us a clear correlation between colour and the shift in value of the manganese, we can see higher values, greater variability and more extremes within the data for the red layering. This is particularly interesting as it draws a line between the shifts in the manganese concentration and depositional cycles.

As discussed in section 1.2, Clift et al., (2014) uses a number of different proxies in order to interpret data on the Chinese monsoon from around 25 Ma. One of the proxies that they utilise for understanding changes in chemical weathering over time is the ratio of K/Rb, with the lower values representing more alteration and thus increased chemical weathering. Figure 13 has one significant

peak at around 325 cm and two less significant peaks around 25 cm and 500 cm. It also has dips in the data around 200 cm, 400 cm and 600 cm. For the K/Rb proxy, a lower value indicates more alteration (Clift et al., 2014). Based on the Clift et al., (2014) interpretation of this ratio we are looking at three significant periods of high chemical weathering (troughs in the data) during the period of this sandstones deposition. Between each of these periods of increased chemical weathering there are significant intervening reductions in chemical weathering (high ratio values at 325 cm). Based on the other factors that we understand from the literature concerning the PAF, the most likely cause of these shifts in chemical weathering is land based glaciers capping the rocks, thus preventing the action of chemical weathering for the duration of the glacial period. While this makes for some compelling data, on its own, without alternate proxies it remains speculative.

Figure 14 shows the plotted concentration of manganese minus light elements against depth for the sandstone. Once more, the colour of the points indicates the distribution of colour throughout the outcrop as cycles of deposition change over time. This data shows several significant fluctuations. The significant peaks in this data occur around 200 cm, 400 cm and 600 cm. Of initial note is the similarity between the spikes in Mn – LE data and the dips in K/Rb data.

As discussed in section 1.2, Jakobsson et al., (2000) used manganese as a proxy in their study of Arctic sediments. It was interpreted in this study as representing an increase in deep water oxygenation due to increased surface ventilation. In the case of the Jakobsson et al., (2000) study this was interpreted as being caused by changes in the distribution of sea ice cover altering ventilation. Based on this proxy, figure 14 combined with the box plot in figure 21 can be interpreted as representing two separate manganese cycles. The first, wider cycle, reflects the long-term cycle of manganese influenced by the shifts in deep water oxygenation whereas the shorter cyclicity is shown most clearly in the box plot, reflecting variations in manganese during deposition on a much shorter scale.

The variations in manganese can thus be established as a proxy for interpreting that 200 cm, 400 cm and 600 cm depth represent significant decreases in ice cover to the ocean at the point of deposition for the PAF. An alternative interpretation to this could also be that the three variations represent shorter timescale fluctuations, as discussed in the previous paragraph, and that in terms of the shift in oxygenation we are looking at a single larger curve in the data. This agrees with the data of the K/Rb (Figure 13) which is a proxy for terrestrial ice cover. Jakobsson et al., (2000) also observe correlation between manganese concentrations and what the study describes as 'dark to medium brown units' due to oxidising conditions.

Figure 20 provides a unified view of the K/Rb and Mn – LE datasets, from this plot it is clear to see that with each notable increase of deep-water oxygenation there is a corresponding increase in the occurrence of chemical weathering in the terrestrial environment. As mentioned previously, these two proxies are complementary, combining to offer a general proxy for glacial ice cover. It would be a rational assumption that the periods in which we see corresponding inverse spikes in the two proxies indicate periods of glaciation, most likely, that occurred closer to the poles than the depositional location, thus explaining the lack of additional diamictite layers at this particular point.

Through the observation and analysis of colour throughout the sandstone we have the most available indicator for cycles of deposition occurring throughout the formation of this sedimentary layer. The shifts back and forth between red and green layers were the reason for the selection of the sandstone and illustrate changes to the chemistry of the source material. When comparing each of the data plots in this analysis to the distribution of colour cycles and so deposition cycles throughout the process of sedimentation the most striking comparison is in the manganese minus light elements plot. This is particularly illustrated with the box plot in figure 21. This plot shows far greater extremes and variability in the red layering when compared to either of the other colour types and far higher maximum values. While this suggests some coupling of the manganese to depositional cycles which are likely controlled by shifts between high and low energy deposition the wider shifts outlined by this study are on a far larger timescale. As such, this correlation between manganese concentration and colour is likely caused by cyclicity of depositional energy whereas the wider shifts in manganese as represented in figure 19 compared against K/Rb show us the less extreme glacial-interglacial shifts occurring outside of the global or near global glacial events.

The large shifts in the data for these proxies across the study of a single interglacial sandstone layer does raise some intriguing questions. The literature and the study illustrated in the sedimentary log in figure 12 suggest that throughout the PAF what we are observing is shifts between glacial and interglacial periods, continuing for some time following the events that occurred during the deposition of the Great Breccia and Disrupted Beds. It seems, therefore, anomalous to have observed indicators of such shifts in glaciation, within a single interglacial layer.

One possible explanation for these data is that we are observing some, previously unnoticed and more minor shifts in glaciation that occurred on much shorter timescales than those observed throughout the glacial to interglacial cyclicity of the main units of the PAF. As such, it is likely that the sedimentary layers were deposited during glacial-interglacial periods with more similarity to more recent ice ages (with glacial ice restricted to polar or near-polar latitudes) whereas the diamictites were deposited under more severe glaciations. We know that this deposition occurred in shallow seas around 30°S

and so this speculation suggests that during even interglacial periods there were some, comparatively very short lived, and yet drastic shifts in climatic conditions.

There are some alternate explanations worth noting for these data. It is conceivable that, in fact, this data represents an unconformity within the archive of this sandstone. At some point during the deposition there may have occurred periods of glacial deposition which has been subsequently eroded prior to further deposition. This would leave the broken record which is potentially what has been studied here, leaving behind the indicators of reductions in chemical weathering and deep ocean oxygenation but not the distinctive diamictite layers that, through study of the wider PAF we would expect to find under such paleo conditions. The obvious issue with this, however, is that the high energy deposit of the diamictite would be the one remaining, making this an unlikely theory. Alternatively, it is possible that the period in question was one without significant deposition to the basin in question during this time. It is possible that the distribution of the ice sheet in question was causing little to no deposition in this area, with a wider distribution set throughout a greater region. If this was the case then we may be able to analyse the product of a brief glacial period, for instance ocean ventilation and a reduction in chemical weathering without the deposition of diamictite that we would generally expect to see. Ultimately, the evidence appears to suggest that glaciation was ongoing, but simply restricted to the polar regions, as we would recognise from more geologically recent glacial periods.

## 6. CONCLUSION

The sedimentary log carried out across the top of the PAF largely confirms previous description as referenced in the literature (Ali et al., 2017; Kilburn et al., 1965; Spencer, 1971) and is interpreted as having distinct cyclicity. The cyclicity can be seen, even from just a cursory examination of the area, shifting between sedimentary deposits and diamictite, arguably, glacial and interglacial deposits.

XRF analysis of the sandstone at Port Askaig showed significant variations against depth in both elemental concentrations and specific proxy ratios derived from the literature. These variations indicate significant shifts in environmental factors contributing to deposition, suggesting, in all likelihood that there is some scale of glaciation missing from the wider archive of the PAF and perhaps occurring over shorter periods than is demonstrable elsewhere.

K/Rb as analysed in ratio displays several shifts in the data, suggesting shifts in the intensity of chemical weathering during the period of deposition. The concentration of manganese within the analysed area also shifts in a similar pattern, reflecting that of the K/Rb. This, according to proxies used by (Jakobsson et al., 2000) suggests shifts in deep ocean oxygenation. As such, it is likely that these data reflect shifts

in glaciation in both the terrestrial and marine environment at polar latitudes, explaining the absence of diamictites during the Neoproterozoic.

## 7. ACKNOWLEDGEMENTS

I would like to thank my supervisor Alasdair Skelton, not just for his support during this project but for his entire approach to teaching, which is a large part of why I have reached this point in the program. My field partner, Maria Strand for her help in gathering the data and for all the laughs while climbing, wading and all-round struggling across the east coast of Islay. Thanks also to Otto Hermelin for making the front-page of my thesis.

My wife Kate I'd like to thank for her endless support, without whom I would never have completed this work or this degree. I would also like to thank Mildred the seal, who kept me company and my spirits high on my darkest day of lonely field work.

Lastly, many thanks to Stockholm University for running such a fantastic program with a wealth of excellent teaching and fieldwork.

## 8. REFERENCES

- Ali, O.D., Spencer, A.M., Fairchild, I.J., et al, 2017, Indicators of relative completeness of the glacial record of the Port Askaig Formation, Garvellach Islands, Scotland: Precambrian Research, <https://doi.org/10.1016/j.precamres.2017.12.005>.
- Ali, D. O. *et al.*, 2017, Indicators of relative completeness of the glacial record of the Port Askaig Formation, Garvellach Islands, Scotland: Precambrian Research, v. 0–1, doi:10.1016/j.precamres.2017.12.005.
- Arnaud, E., Eyles, C. H., 2002, Catastrophic mass failure of a Neoproterozoic glacially influenced continental margin, the Great Breccia, Port Askaig Formation, Scotland: Sediment. Geol., v. 151, p. 313–333.
- Arnaud E., Fairchild I.J., 2011, The Port Askaig Formation, Dalradian Supergroup, Scotland: Memoirs of the Geological Society of London, v. 36, p. 635-642.
- Benn, D. I., Prave, A. R., 2006, Subglacial and proglacial glacitectonic deformation in the Neoproterozoic Port Askaig Formation, Scotland: Geomorphology, v. 75, p. 266–280.
- Chew, D.M., Strachan, R.A., 2014. The Laurentian caledonides of Scotland and Ireland. In: Corfu, F., Gasser, D., Chew, D.M. (Eds.), *New Perspectives on the Caledonides of Scandinavia and Related Areas*. 390. Geological Society, London, Special Publication, p. 45–91.
- Deynoux, M., 1985, Terrestrial or waterlain glacial diamictites? Three case studies from the Late Precambrian and Late Ordovician glacial drifts in West Africa: Palaeogeography, Palaeoclimate, Palaeoecology, v. 51, p. 97–141.
- Evans, D.A.D., 2000. Stratigraphic, geo-chronological, and paleomagnetic constraints upon the Neoproterozoic climatic paradox: *Am. J. Sci.*, v. 300, p. 347–433.
- Fairchild, I. J. *et al.*, 2017, Tonian-Cryogenian boundary sections of Argyll, Scotland: Precambrian Res, 1–28. doi:10.1016/j.precamres.2017.09.020
- Fairchild, I. J. & Kennedy, M. J., 2007, Neoproterozoic glaciation in the Earth System: *J. Geol. Soc. London*, v. 164, p. 895–921.
- Hoffman, P. F. *et al.*, 2017, Snowball Earth climate dynamics and Cryogenian: *Sci. Adv.* v. 3.
- Hoffman, P. F. & Schrag, D. P., 2002, The snowball Earth hypothesis: testing the limits of global change: *Terra*, v. 14, p. 129–155.

- Hoffman, P.F. and Schrag, D.P., 2000. Snowball Earth: *Sci. Am.*, v. 282, p. 62–75.
- Hoffman, P. F., 1998, A Neoproterozoic Snowball Earth: *Science*, v. 281, p. 1342–1346.
- IPCC Data, 2018, What is a GCM?. [ONLINE] Available at: [http://www.ipcc-data.org/guidelines/pages/gcm\\_guide.html](http://www.ipcc-data.org/guidelines/pages/gcm_guide.html). [Accessed 2 May 2018].
- James, N. P., Narbonne, G. M. & Kyser, T. K., 2001, Late Neoproterozoic cap carbonates, Mackenzie Mountains, northwestern Canada, Precipitation and Global Glacial Meltdown: *Can. J. Earth Sci.*, v. 38, p. 1229–1262.
- Karhu, J. a & Holland, H. D., 1996, Carbon isotopes and the rise of atmospheric oxygen: *Geology*, v. 24, p. 867–870.
- Kilburn, C., Pitcher, W.S., Shackleton, R.M., 1965. The stratigraphy and origin of the Port Askaig Boulder Bed Series (Dalradian): *Geol. J.*, v. 4, p. 343–360.
- Kirschvink, J.L., 1992, Late Proterozoic low-latitude global glaciation the snow- ball earth: *The Proterozoic Biosphere* (J. W. Schopf and C. Klein, eds), p. 51–52.
- Lewis, J.P., Weaver, A. J., Eby, M., 2007, Snowball versus slushball Earth: Dynamic versus nondynamic sea ice: *J. Geophys. Res.*, v. 112, C11014.
- Macdonald, F. A. *et al.*, 2010, Supporting Online Material for Calibrating the Cryogenian: *Group*, v. 1241, p. 1241–1244.
- Ogg, J.G., G., Gradstein, F.M., 2016, *A Concise Geologic Time Scale*, Elsevier, ISBN: 978-0-444-63771-0.
- Palmer, P.T., 2011. Energy-Dispersive X-ray Fluorescence spectrometry A long overdue addition to the chemistry curriculum: *J. Chem. Educ.*, v. 88, p. 868–872, <https://doi.org/10.1021/ed200254v>.
- Pierrehumbert, R. T., 2005, High levels of atmospheric carbon dioxide necessary for the termination of global glaciation: *Nature*, v. 429, p. 646–649.
- Prave, A.R., Fallick, A.E., Thomas, C.W. & Graham, C.M., 2009, A composite C-isotope profile for the Neoproterozoic Dalradian Supergroup of Scotland and Ireland: *J. Geol. Soc. London*, v. 166, p. 845–857.
- Rice, A.H.N., Hofmann, C.C., 2000, Evidence for a glacial origin of Neoproterozoic III striations at Oaibaccann- jar'ga, Finland, northern Norway: *Geol. Mag.*, v. 137, p. 355–366.

Rooney, A.D., Strauss, J.V., Brandon, A.D., Macdonald, F.A., 2015. A Cryogenian chronology: two long-lasting synchronous Neoproterozoic glaciations: *Geology*, v. 43, p. 459–462.

Schermerhorn, L.J.G., 1974. Late Precambrian mixtites: glacial and/or non-glacial: *American Journal of Science*, v. 274, p. 673–824.

Schrag, D.P., Berner, R.A., Hoffman, P.F., Halverson, G.P., 2002, On the initiation of a snowball Earth: *Geochemistry, Geophysics, Geosystems*, v. 3, p. 1–21.

Spencer, A.M., 1971, Late Pre-Cambrian glaciation in Scotland: *Memoirs of the geological Society*, London, v. 6.

Spencer, A.M., Spencer, M.O., 1972, The Late Precambrian/Lower Cambrian Bonahaven Dolomite of Islay and its stromatolites: *Scottish Journal of Geology*, v. 8, p. 269-282.

User Manual Delta™ Family: Handheld XRF Analyzers. (2010, June). Retrieved on the date August 11, 2018, from <https://usenvironmental.com/download/manuals/Olympus - Delta User Manual.pdf>

Worsley, T.R., Kidder, D.L., 1991, First-order coupling of paleogeography and CO<sub>2</sub> with global surface temperature and its latitudinal contrast: *Geology*, v. 19, p. 1161–1164.

Webster, D., Anderton, R., Skelton, A., 2015, *A guide to the Geology of Islay – An introduction to Islay’s geological past with 12 illustrative walking excursions*, Ringwood Publishing, Glasgow, ISBN 978-1-901514-16-2.